

UNIVERSITY OF VAASA

SCHOOL OF TECHNOLOGY AND INNOVATIONS

ELECTRICAL ENGINEERING

Olli Lamminen

**DEVELOPMENT OF A PERMANENT MAGNET ASSISTED SYNCHRONOUS
RELUCTANCE MOTOR**

Master's thesis for the degree of Master of Science in Technology submitted for inspection

Vaasa, February 23th, 2018

Instructor

Docent Jere Kolehmainen

Supervisor

Professor Timo Vekara

PREFACE

This master's thesis is written for ABB Oy, Motors and Generators in Vaasa, Finland. I would like to thank, Dr. Jouni Ikäheimo, manager of innovation and new technology, for giving me the opportunity to write about this interesting subject and from his good advices during the end of writing process. Special thanks to my instructor Dr. Jere Kolehmainen for the support and guidance throughout the writing process. I would also like to thank all the innovation and new technology team from guidance for the subject, the staff at factory from manufacturing the prototype and the staff at test field from the measurement results.

I would like to thank my supervisor Professor Timo Vekara from Vaasa University, for his good advices and support during the writing process and for the academic support during my studies.

Also, I would like to thank all my fellow students from memorable years of study.

Warmest thanks for all the support I have got throughout my studies to my family and especially to Susanna.

Vaasa, February 23th, 2018.

Olli Lamminen

CONTENTS

PREFACE	2
CONTENTS	3
LIST OF SYMBOLS AND ABBREVIATIONS	5
ABSTRACT	8
TIIVISTELMÄ	9
1 INTRODUCTION	10
2 SYNCHRONOUS MOTORS	12
2.1 Load types of synchronous motors	13
2.2 Permanent magnet motor	14
2.3 Synchronous reluctance motor	15
2.4 Permanent magnet assisted synchronous reluctance motor	16
2.5 Torque production of PMSynRM	18
2.6 Efficiency and losses of PMSynRM	22
2.7 Temperature rise and insulation classes of electric motors	24
2.8 Effect of temperature to permanent magnet material demagnetization	25
3 ABB HIGH DYNAMIC PERFORMANCE SERIES MOTORS	28
4 PROTOTYPE DESIGN OF PMSYNRM	31
4.1 Design method of PMSynRM	32
4.2 Rotor parametrization of PMSynRM	34
5 SIMULATION RESULTS USING ADEPT FCSMEK	38
5.1 Current and power factor of PMSynRM and IM	40
5.2 Losses and efficiency of PMSynRM and IM	40
6 MANUFACTURING PROSESS OF PMSYNRM PROTOTYPE	45
6.1 Rotor electric steel sheet and rotor endplates manufacturing	46
6.2 Rotor core assembly	48
6.3 Shaft assembly in to the rotor core	51
6.4 Rotor magnet assembly	52
6.5 Rotor magnetic forces effect on assembly process	57
6.6 Magnetic rotor assembly inside the stator with special assembly tools	63
7 METHODS AND RESULTS USED IN PROTOTYPE MEASUREMENT	66
7.1 Measurement methods and results of PMSynRM and IM	67
7.2 PMSynRM voltage, current and torque	69

7.3	Efficiencies and temperature rises of PMSynRM and IM	70
8	COMPARISON OF MEASUREMENT AND SIMULATION RESULTS	76
8.1	Open circuit voltage of HDP 250 PMSynRM	76
8.2	Losses and efficiencies of HDP 250 PMSynRM	77
8.3	Power factor and current of HDP 250 PMSynRM	79
9	SUMMARY AND DISCUSSION	81
	REFERENCES	85
	APPENDICES	91

LIST OF SYMBOLS AND ABBREVIATIONS

Greek symbols

α	Temperature coefficient of remanence
δ	Load angle
η	Efficiency
η_{acs}	Efficiency of frequency converter
η_{mot}	Efficiency of electric motor
η_{tot}	Total efficiency of electric motor and frequency converter
$\theta_{Cu,max}$	Maximum stator winding temperature rise
θ_{db}	D-end bearing temperature rise
θ_{fr}	Frame temperature rise
θ_{rt}	Rotor core surface temperature rise
μ_0	Permeability of vacuum
μ_r	Relative permeability of a material
ω	Angular velocity

Other symbols

B	Magnetic flux density
B_k	Magnetic flux density at the knee point of the demagnetization curve
B_n	Magnetic flux density in normal direction
B_r	Magnetic remanence
$B_r, 20\text{ }^\circ\text{C}$	Magnetic remanence at 20 °C
f	Frequency
H	Magnetic field strength
H_c	Magnetic coercivity
I	Electric current
L_d	Direct axis inductance
L_q	Quadrature axis inductance
n	rotational speed
p	Number of poles

P	Power
P_{add}	Additional losses
P_{Cur}	Rotor Joule losses
P_{Cus}	Stator Joule losses
P_{Fer}	Rotor iron losses
P_{Fes}	Stator iron losses
P_{fw}	Mechanical losses
P_{in}	Input power
P_{loss}	Total losses
P_{out}	Output power
R	Resistance
S	Surface area
T_e	PMaSynRM torque production
T_{mag}	Magnetic torque
T_{mech}	Mechanical torque
T_{rel}	Reluctance torque
U	Voltage
U_{acs}	Frequency converter supply voltage
U_{mot}	Motor supply voltage of
U_{oc}	Open circuit voltage
$U_{\text{oc}, 20\text{ }^\circ\text{C}}$	Open circuit voltage at 20 °C temperature
Q	Total number of stator slots

Abbreviations

AC	Alternating current
d -axis	Direct axis
DC	Direct current
D-end	Drive end of motor
DOL	Direct online
DTC	Direct torque control
FC	Frequency converter

FEM	Finite element method
HDP	High dynamic performance
IEC	International Electrotechnical Commission
IM	Induction motor with squirrel cage
IP	Ingress protection
IPMM	Interior permanent magnet motor
ISO	International Organization for Standardization
MAF	Magnetic assembly force
NdFeB	Neodymium iron boron magnet
N-end	Non-drive end of motor
PM	Permanent magnet
PMaSynRM	Permanent magnet assisted synchronous reluctance motor
PMM	Permanent magnet motor
q -axis	Quadrature axis
SM	Synchronous motor
Sm ₂ Co ₁₇	Samarium cobalt
SPM	Surface mounted permanent magnet motor
SynRM	Synchronous reluctance motor
UMP	Unbalanced magnetic pull
VSD	Variable speed drive

UNIVERSITY OF VAASA**School of Technology and Innovations**

Author:	Olli Lamminen
Topic of the Thesis:	Development of a Permanent Magnet Assisted Synchronous Reluctance motor
Instructor:	Docent Jere Kolehmainen
Supervisor:	Professor Timo Vekara
Degree:	Master of Science in Technology
Major of Subject:	Electrical Engineering
Year of Entering the University:	2009
Year of Completing the Thesis:	2018

Pages: 94

ABSTRACT

This thesis is a development research project for a permanent magnet assisted synchronous reluctance motor (PMaSynRM) used with frequency converter (FC). The motor size is specified to International Electrotechnical Commission (IEC) with frame size 250. The objective of this thesis is to develop air-cooled high dynamic performance (HDP) series motor with PMaSynRM rotor technology. The PMaSynRM designing goals are good thermal behavior and high efficiency at wide speed range with a wide field weakening area.

To study the objectives of this thesis a prototype of PMaSynRM is designed and manufactured. The designed prototype of PMaSynRM is investigated with simulations and measurements at different operating points on a load type of constant torque and constant power with wide field weakening area. The performance values of PMaSynRM prototype rotor is compared with simulations and measurements to an induction motor's (IM's) rotor which is earlier manufactured and measured in the same HDP 250 stator.

The simulation and measurement results showed that PMaSynRM has benefits on thermal behavior and efficiency compared to IM. PMaSynRM measured operating points at constant torque from running speed 525 rpm to 1050 rpm and at constant power from 1050 rpm to 3000 rpm showed that PMaSynRM is well suitable to operate in wide speed range because of wide field weakening area.

PMaSynRM simulation and measurement results had a bit difference on the efficiencies because the Adept FCSmek simulation tool does not take into account the high level of supply harmonics outside field weakening area which are produced from frequency converter. The prototype of PMaSynRM reached to higher output level than the IM because of good thermal behavior. The PMaSynRM also met the expectations on high efficiency on a wide field weakening area.

KEYWORDS: Permanent magnet assisted, synchronous reluctance motor, manufacturing process, wide speed range motor, wide field weakening area

VAASAN YLIOPISTO
Tekniikan ja innovaatiojohtamisen yksikkö

Tekijä:	Olli Lamminen	
Diplomityön nimi:	Kestomagneettiavusteisen tahtireluktanssimoottorin kehittäminen	
Ohjaaja:	Dosentti Jere Kolehmainen	
Valvoja:	Professori Timo Vekara	
Tutkinto:	Diplomi-insinööri	
Oppiaine:	Sähkötekniikka	
Opintojen aloitusvuosi:	2009	
Diplomityön valmistumisvuosi:	2018	Sivumäärä: 94

TIIVISTELMÄ

Tässä diplomityössä keskityn taajuusmuuttajakäyttöisen kestopagneettiavusteisen tahtireluktanssimoottorin (*eng. permanent magnet assisted synchronous reluctance motor, PMaSynRM*) suunnitteluun, valmistamiseen ja koekäyttöön. Moottorin runkokoko on määritetty kansainvälisen sähköalan standardointiorganisaation mukaan 250-runkokoon moottoriksi. Diplomityöni tavoite on kehittää (*eng. high dynamic performance, HDP*) -sarjan 250-runkokokoinen moottori PMaSynRM-roottorilla. PMaSynRM-roottorin suunnittelun tavoitteina on saavuttaa matala lämpenemä sekä korkea hyötysuhde laajalla pyörimisnopeusalueella sekä pitkällä kentänheikennysalueella.

PMaSynRM-roottorin toimintapisteiden suoritusarvoja tutkitaan simulointiohjelman avulla ja verrataan samassa staattorissa käytettyyn oikosulkuroottorin simuloituihin arvoihin. PMaSynRM-prototyyppi roottori suunnitellaan ja valmistetaan HDP 250-rungon staattoriin ja sen mitattuja arvoja verrataan jo aiemmin valmistettuun oikosulkuroottoriin, joka on koeajettu samalla staattorilla. PMaSynRM prototyyppi koeajetaan eri toimintapisteissä vakiomomentilla ja vakioteholla sekä laajalla kentänheikennysalueella.

Simulointi- ja mittaustulokset osoittivat, että PMaSynRM-roottori saavuttaa matalamman lämpenemän ja korkeamman hyötysuhteen kuin oikosulkuroottori. PMaSynRM:n mittaukset suoritettiin vakioteholla pyörimisnopeudella 525–1050 rpm ja vakiomomentilla pyörimisnopeudella 1050–3000 rpm. PMaSynRM:n mittaustulokset vakiomomentilla ja vakioteholla osoittivat, että moottori soveltuu hyvin käytettäväksi laajalle nopeusalueelle pitkän kentänheikennysalueen ansiosta.

Hyötysuhteiden osalta PMaSynRM:n simulointi- ja mittaustuloksissa oli hieman eroavaisuuksia mikä johtui siitä, että Adept FCSmek -simulointiohjelma ei ota huomioon taajuusmuuttajan aiheuttamia harmonisia yliaaltoja kentänheikennysalueen ulkopuolella. PMaSynRM:ia pystyttiin ajamaan suuremmalla teholla kuin oikosulkumoottoria matalan lämpenemän vuoksi. PMaSynRM saavutti odotusten mukaisesti myös korkean hyötysuhteen laajalla kentänheikennysalueella.

KEYWORDS: Kestomagneettiavusteinen, synkronireluktanssimoottori, valmistusprosessi, laajan nopeusalueen moottori, pitkä kentänheikennysalue

1 INTRODUCTION

High energy efficient products are in a major role when discussing about energy saving. In developed countries, more than 50 % of the produced electricity is used in electric motors and about 60–80 % of these electric motors are used in the industrial section and 35 % in the tertiary sector. Three-phase alternating current (AC) motors are the most common motor type in industrial section. They can be divided in subgroups of synchronous and asynchronous motors. The most conventional three-phase AC motor used in industrial applications is asynchronous squirrel cage induction motor (IM), which can be used direct online (DOL) and in variable speed drive (VSD) applications.

To improve electric motors energy efficiency, International Electrotechnical Commission (IEC) has set up efficiency standard IEC/EN 60034-30-1. Even though the purchasing price of high efficiency motors may be high, it has been investigated that the costs during motor life-cycle span can consist 97 % from electric energy consumption (Vesti 2013: 10), which means that energy efficient electric motors have lower costs during life-cycle. Synchronous motors which can be operated only in VSD applications do not yet have any efficiency regulations.

Development of power electronic devices such as frequency converters (FCs), has enabled more energy efficient use of synchronous motors in VSD applications, especially if compared to the early days when synchronous motors were designed with squirrel cage. (Haataja 2003: 15). Nowadays advanced converters enable synchronous motors to produce the starting torque without a squirrel cage. However, converter-feed has disadvantages on increasing the additional losses in the motor, which are affected from the converter's supply harmonics. Even though additional losses decrease the motor efficiency, the total energy consumption is often lower in VSD applications than in DOL applications because of the speed adjust according to the load (Kärkkäinen, Aarniovuori, Niemelä, Pyrhönen 2017: 45–46; Mohanarajah, Rizk, Nagrial, Hellany 2016: 1).

Let us review more closely the three-phase synchronous motors used in VSD applications. There are three subgroups which are separately excited synchronous motors (SMs),

permanent magnet motors (PMMs) and synchronous reluctance motors (SynRMs). In this thesis, the SMs are excluded from the review. Combination of PMM and SynRM can be called as a permanent magnet assisted synchronous reluctance motor which has many abbreviations, but in this master's thesis PMSynRM is used. In VSD applications the PMSynRM is an interesting alternative for the most conventional IM. Both motors have a wide constant power speed range but PMSynRM has claimed to have advantages on electrical and thermal behaviour (Kolehmainen 2017: 4; Fratta, Vagati, Villata 1992: 702–703.)

This thesis is based on a PMSynRM prototype development research project, done for the low voltage motor manufacturing company ABB Oy, Motors and Generators, Vaasa Finland. The main topic of this thesis is to introduce a prototype development process and methods. A comparison between PMSynRM and the most conventional IM properties is reviewed with a literature study and from simulation and measurement results. PMSynRM rotor is designed to ABB's high dynamic performance (HDP) series stator which are through ventilated stators (ABB 2015a: 59). IM with aluminium squirrel cage has been previously tested in the HDP stator. Size of the prototype HDP motors is specified in International Electrotechnical Commission (IEC) with frame size 250.

Chapter 2 deals with introduction to synchronous motors and to PMSynRM structure and operating principle. Chapter 3 has introduction for HDP series motor structure, most common applications and comparison to the ABB's Process Performance series motor. Chapter 4 introduces the basics of electric motor designing which is important to know when developing a prototype. Chapter 5 focuses on PMSynRM prototype simulations and also PMSynRM and IM simulation results are compared. In Chapter 6 the prototype manufacturing methods are presented and explained. In Chapter 7 the measurement methods are explained and the results are presented. Chapter 8 presents comparison of simulation and measurement results. Finally, in chapter 9 are conclusions presented.

2 SYNCHRONOUS MOTORS

Electric three-phase AC motors can be divided in synchronous and asynchronous motors. Synchronous motors are called as synchronous, because the rotor velocity follows the stator rotating magnetic field velocity in absolute synchronism. Whereas in the asynchronous motors rotor velocity and stator rotating magnetic field velocity has a slip between. Synchronous motors have two major types based to the rotor magnetization which are non-excited and direct current (DC) excited. In Figure 1 is a classification of electric three-phase AC motors that are reviewed in this thesis.

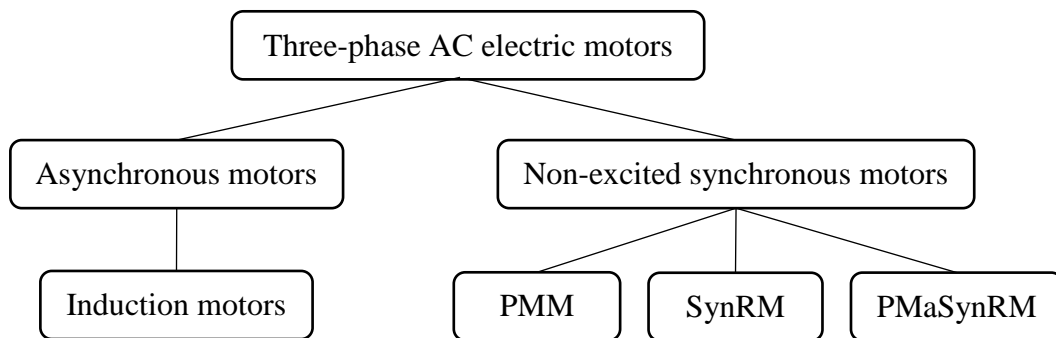


Figure 1. Classification diagram of three-phase AC electric motors.

The major type of motors used in industrial sector are asynchronous IMs of squirrel cage type. Non-excited synchronous motors are also used in industrial sector and the two main types are PMMs and SynRMs. PMaSynRM is also a non-excited synchronous motor and it can be said that it is a combination of SynRM and PMM. The main difference between synchronous and asynchronous motors are the operational principle and the rotor structure. Both, synchronous and asynchronous motors may use same kind of wound stators. (Pyrhönen, Jokinen, Hrabovcova 2014: 342, 388–389; Aura & Tonteri 1996: 323–325.) The non-excited synchronous motors are studied more on the next chapters.

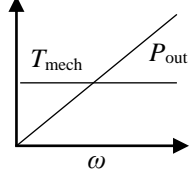
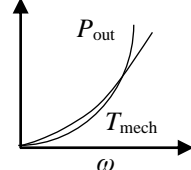
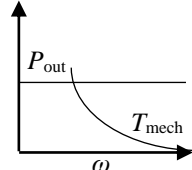
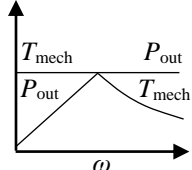
2.1 Load types of synchronous motors

The use of synchronous motors can be divided in four common load types as constant torque, quadratic torque, constant power and constant power/torque. Table 1 presents the different common load types with the function of running speed. Output power P_{out} , mechanical torque and running speed are directly proportional on each other's as

$$P_{out} = T_{mech} \cdot \omega, \quad (1)$$

where, T_{mech} is mechanical torque and ω refers to running speed as shaft angular velocity.

Table 1. Common load types, applications and load curves of synchronous motors. Modified from (Kolehmainen 2011: 25).

	Constant torque	Quadratic torque	Constant power	Constant power/torque
Applications	Conveyors, feeders and screws	Centrifugal pumps and fans	Rollers	Paper machine rolls and electric vehicles
Load curve				

Constant torque is typically used in such applications as conveyors, feeders, screws and compressors. Quadratic torque is used typically in pumps and fans and constant power is typically used in roller applications. Paper machines and electric vehicles utilize a combination of constant torque and constant power (Kolehmainen 2011: 25). In this thesis the prototype of PMASynRM is designed to be used in constant torque and constant power with a wide field weakening area.

2.2 Permanent magnet motor

Major of the PMM torque production bases on permanent magnets and minor on magnetic reluctance. PMMs have a similar stator as IMs but there are lot of differences in the rotors because PMM rotor is structured with permanent magnets and there is no squirrel cage. There are different types of PMM rotors which can be classified with the magnet mounting position as presented in Figure 2, where the surface mounted magnet rotor (a) has a simple structure, which makes it easy to manufacture. This type of rotor is not well suited for high rotational speeds because the magnets are not well protected mechanically or magnetically. In inset mounted magnet rotor (b) the magnets are better protected compared to surface mounted magnets. Embedded mounted magnet rotors (c) and (d) have well protected magnets inside the rotor slots. Embedded mounted magnet rotors are also called in literature as internal permanent magnet rotors (IPMM) (Kolehmainen 2011: 19–20; Hirvelä 2013: 10).

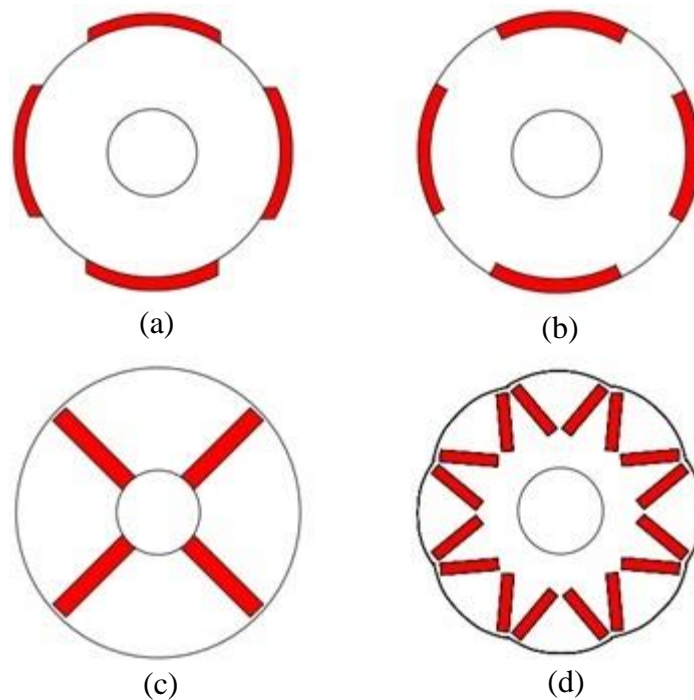


Figure 2. Various permanent magnet rotor two-dimension geometries where rotor has surface mounted magnets (a); inset mounted magnets (b); radially embedded mounted magnets (c); V position embedded mounted magnets (d). Modified from (Salminen 2004: 23).

Comparing equal size surface mounted magnet rotor to that of IPMM, the IPMM needs a larger volume of magnet material to reach on equal output power (Salminen 2004: 23). However, eddy currents are smallest in IPMM rotors compared to surface mounted and inset mounted rotors. Also embedded mounted magnets increase the rotor flux by concentrating it (Kolehmainen 2011: 19). Benefits of PMMs are generally a very high efficiency and very high torque production. (Mohanraja 2016: 5; Pyrhönen etc. 2014: 427–429.) Disadvantage of PMMs are high manufacturing cost because of the high price of permanent magnet material. PMMs have a limited field weakening area so it is not suitable to be used in high speed range applications (Kolehmainen 2017: 4; Hirvelä 2013: 10). PMMs use is popular in low-speed and high-torque applications. In industrial use PMMs are most commonly operating in pumps, fans, compressors, mills, hoists and transportation systems (Gieras 2002: 17–18).

2.3 Synchronous reluctance motor

SynRM torque production bases only on reluctance torque. When SynRM is designed for VSD use, the rotor does not need a squirrel cage and it is simple to manufacture. Three major types of four-pole SynRM rotor designs are presented in three-dimensions in Figure 3, which are radially laminated simple salient pole rotor (a), axially laminated rotor (b) and radially laminated rotor with flux barriers (c).

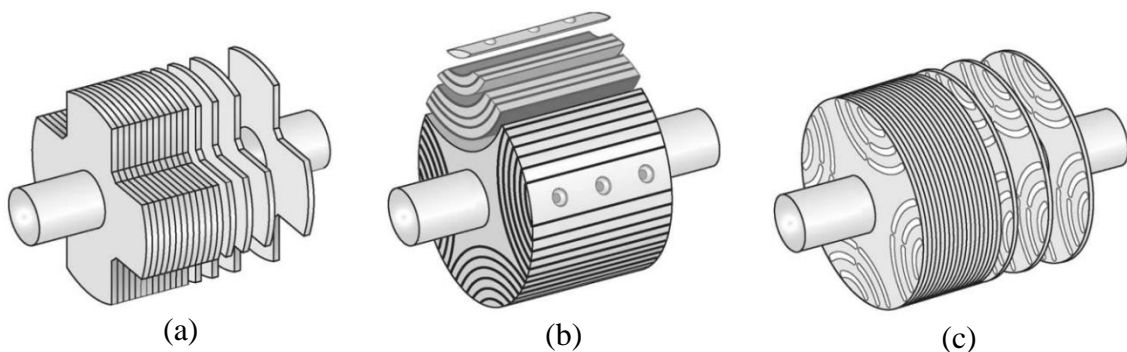


Figure 3. SynRM rotors geometries, radially laminated simple salient pole rotor (a), axially laminated rotor (b) and radially laminated rotor with flux barriers (c) (Kolehmainen 2011: 18).

The radially laminated simple salient pole rotor is easy to manufacture because it has simple and robust design, but it has also a poor performance because of low saliency ratio. Four-pole axially laminated rotor is challenging to manufacture because of its complex design. The axially laminated rotor has a good performance because of good saliency ratio, but it has high eddy current losses because of axial direction lamination. Radially laminated rotor with flux barriers has good performance, it is simple to manufacture and the eddy current losses are small (Kolehmainen 2011: 18).

The stator of SynRM is similar as that in IMs (Mohanrajah 2016: 1). SynRM is a great choice for industrial VSD applications when high efficiency is demanded for a wide speed range. SynRMs are used for example in pumps, fans, compressors, conveyors, mixers and extruders (ABB 2016: 6). SynRM has high efficiency and high torque density when compared to IM, and it is also potentially cheaper to manufacture in mass production. SynRM can be highly overloaded because of low rotor temperature rise. Lower rotor temperature is an affecting factor for motor reliability and lifetime. Disadvantage of SynRM compared to IM is a poor power factor which affects that the frequency converter needs to be oversized (Hirvelä 2013: 10; Moghaddam 2011: 22–23, 38, 100).

2.4 Permanent magnet assisted synchronous reluctance motor

During the last decades, there has been large interest for PMSynRMs in different research and development projects. PMSynRM torque production bases partly on magnetic reluctance and partly on permanent magnets. Adding permanent magnets in SynRM rotor's flux barriers the power factor can be increased. The PMSynRM rotor can be designed for example with a small volume of high quality permanent magnets (PMs) or with a larger volume of low cost PMs, as the both options are cheaper to manufacture than PMM rotor (Moghaddam 2011: 55–57). PMSynRM rotors have been manufactured with different design specifications that varies for example on number of flux barriers, width and shape of flux barriers, magnetic material, magnet placements and volume of magnets. Alternative designs of PMSynRM rotors are presented in Figure 4.

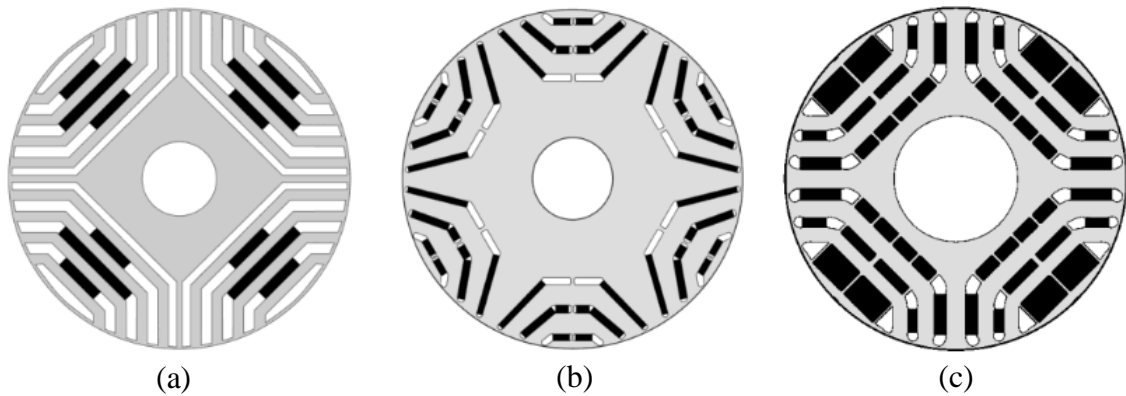


Figure 4. Alternative PMSynRM two-dimension rotor geometries where the smallest amount of magnets are ferrite magnets (a), neodymium magnets (b) and the largest amount of magnets are samarium cobalt magnets (c). Modified from (Hirvelä 2013: 87–89).

In Figure 4a can we see that rotor with ferrite magnets is a four-pole rotor and it has five flux barriers. In one pole, three of the five flux barriers are designed to have magnets. Neodymium magnet rotor in Figure 4b is six-pole rotor and it has three flux barriers in each pole and all of them have neodymium magnets. Rotor with samarium cobalt magnets in Figure 4c, again is a four-pole rotor and there are three flux barriers per pole which all have magnets. In the neodymium magnet rotor and samarium cobalt magnet rotor bridges can be seen across the flux barriers which are used to increase the rotors a mechanical strength. More alternatives of PMSynRM rotor geometries can be find from (Hirvelä 2013: 87–89).

PMSynRM has high efficiency, high power factor and high power density if compared to SynRM but the rotor manufacturing costs are also higher because of the of PM material. PMSynRM benefits compared to PMM is the capability to operate in high speed applications and lower manufacturing costs. Disadvantages of PMSynRM compared to PMM is a lower efficiency and power density. If PMSynRM is compared to conventional IM, both are suitable for wide speed range operation but PMSynRM has better efficiency and power density. (Kim, Kim, Kim, Kang, Go, Chun, Lee 2009: 4660; Kolehmainen 2017: 4.)

2.5 Torque production of PMSynRM

Electric motor rotates when the produced magnetic torque become higher than the mechanical counter torque. The electric motor magnetic torque in air gap is affected from the magnetic circuit of stator and rotor. PMSynRM torque production bases partly on properties of SynRM and partly on properties of IPMM (Moghaddam 2011: 55).

Reluctance torque production

Rotor and stator steel sheets are made of soft ferromagnetic material which is also called as non-magnetized material or electrical steel. Soft ferromagnetic materials have low reluctance so they easily magnetize in external magnetic field. Soft ferromagnetic material also strengthens the magnetic flux density. In Figure 5 is presented magnetization curves, also called as B - H curves for steel, iron and air. From Figure 5 we can note different material properties on flux density B production in external magnetic field H . Also, the magnetic material saturation with the function of magnetic field's strength can be noted.

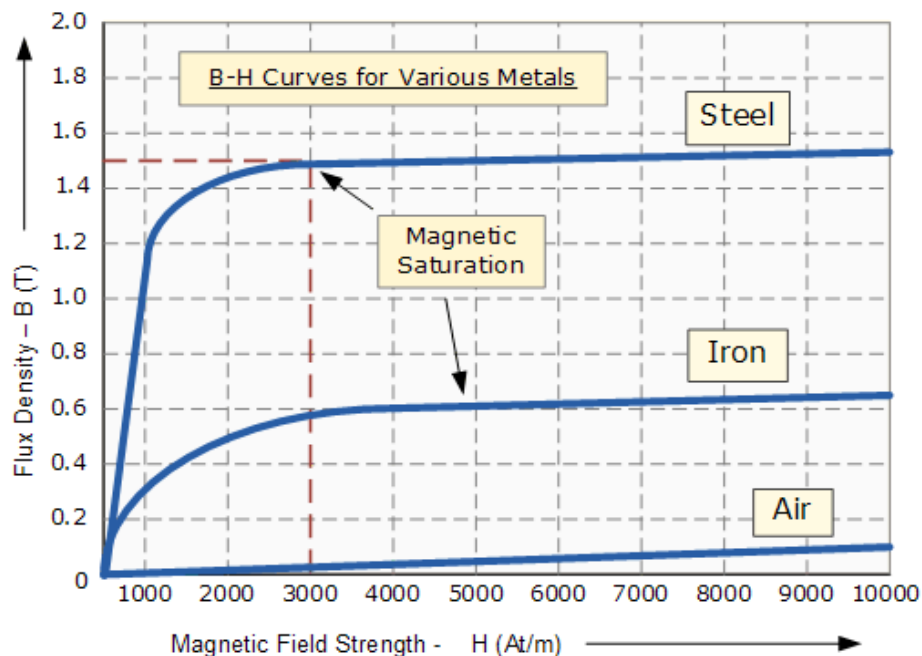


Figure 5. Magnetization or B - H curves of steel, iron and air (Electronic tutorials).

When a soft ferromagnetic object, for example a steel plate, is placed asymmetrically in external uniform magnetic field, it is first magnetized and then the magnetic field tries to align the magnetized object on the same direction. Figure 6 presents the force effect between asymmetrically placed soft ferromagnetic rectangular object and uniform magnetic field.

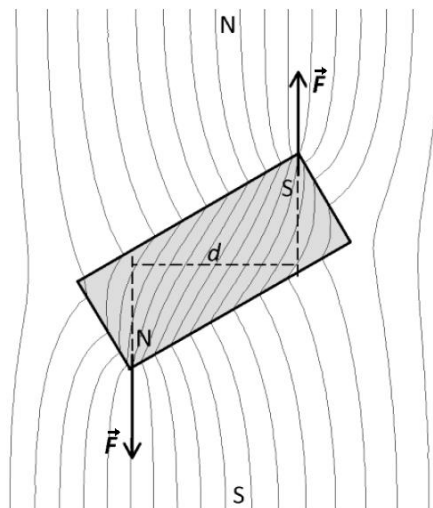


Figure 6. Torque produced on asymmetrically placed soft ferromagnetic rectangular object in a uniform magnetic field. Modified from (Hirvelä 2013: 23).

The rectangular object presented in Figure 6 can be one of the multiple flux routes beside flux barriers as for example air, in the reluctance motor's rotor core. The flux routes and flux barriers are presented in Figure 7. Electromagnetic torque in SynRM consists only on reluctance torque (Haataja 2013: 19), which is produced in the air gap of stator and rotor core (Hirvelä 2013: 16–25; Kolehmainen 2012b: 2–5.)

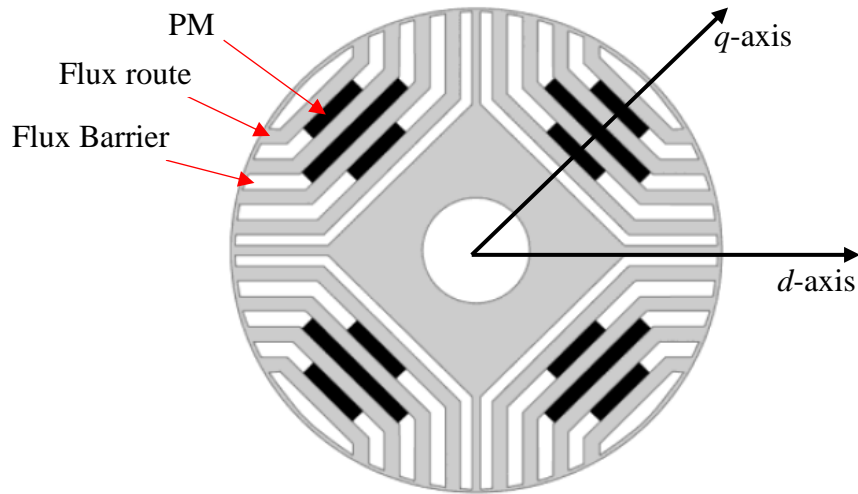


Figure 7. Example of a PMSynRM rotor core two-dimension drawing. Modified from (Hirvelä 2013: 87).

Permanent magnet torque production

Permanent magnet material in external magnetic field has similar force effect as magnetized ferromagnetic object but with the difference that permanent magnet object is already magnetic, without need of external field magnetization. Embedded magnets inside the rotor core cannot rotate freely so the torque production bases majorly on unusually shaped magnetic field created from the attraction of PMs and rotor core. Permeability of permanent magnet material is close to permeability of air, so the magnets placements are proportional to the flux barriers in SynRM rotor. Permanent magnet material placement in IPMM rotor creates flux barriers which strengthens the IPMM also to produce reluctance torque. (Haataja 2003: 21; Hirvelä 2013: 22–25.)

PMSynRM rotor geometry presented in Figure 7 can be divided in two different axes regarding the magnetic flux direction. Direct axis (d -axis) produces the major flux of the rotor in the flux routes direction and quadrature axis (q -axis) produces the minor flux. In SynRMs the d -axis and q -axis are presented exactly as in PMSynRMs. In PMMs the axes are mostly determined oppositely as compared to SynRMs and PMSynRMs. In PMM the d -axis is orthogonally to the direction of major flux production by permanent magnets and q -axis in minor flux direction (Hirvelä 2013: 14–15; Moghaddam 2011: 57).

PMSynRM torque production can be presented with combination of reluctance and magnetic torque when the d -axis and q -axis inductances and permanent magnets induced voltage are known. The PMSynRM torque production bases majorly on reluctance torque

$$T_{\text{rel}} \approx \frac{3}{2} \frac{p}{\omega} \left(\frac{\hat{u}_s^2}{2} \left(\frac{1}{L_q \omega} - \frac{1}{L_d \omega} \right) \sin 2\delta \right), \quad (2)$$

where p is motor pole pair number, \hat{u}_s is stator voltage, L_d is direct axis inductance, L_q is quadrature axis inductance and ω is angular velocity. δ is load angle between stator voltage and rotor q -axis. The minor of PMSynRM torque production bases on magnetic torque produced by permanent magnets. The magnetic torque in d -axis direction can be presented with surface mounted permanent magnet motor (SPM) torque production

$$T_{\text{mag}} \approx \frac{3}{2} \frac{p}{\omega} \left(\frac{\hat{u}_p \hat{u}_s}{L_q \omega} \sin \delta \right), \quad (3)$$

where \hat{u}_p is voltage induced by permanent magnets. As the PMSynRM produces majorly reluctance torque T_{rel} and minor magnetic torque T_{mag} , the PMSynRM torque production T_e can approximately be presented as

$$T_e \approx \frac{T_{\text{mag}}}{2} + T_{\text{rel}}, \quad (4)$$

which is more precisely

$$T_e \approx \frac{3}{2} \frac{p}{\omega} \left(\left(\frac{1}{2} \frac{\hat{u}_p \hat{u}_s}{L_q \omega} \sin \delta \right) + \left(\frac{\hat{u}_s^2}{2} \left(\frac{1}{L_q \omega} - \frac{1}{L_d \omega} \right) \sin 2\delta \right) \right) \quad (5)$$

(Kolehmainen 2017: 12–19; Kolehmainen 2012b: 12–14; Salminen 2014: 58.)

2.6 Efficiency and losses of PMSynRM

One of the most important design parameters of electric motors is efficiency which can be defined as

$$\eta = \frac{P_{\text{out}}}{P_{\text{in}}}, \quad (6)$$

where P_{in} is the measured input power and P_{out} is the output power measured from the shaft. Single-phase and three-phase electric motors in DOL use operated with single speed, are defined with efficiency class standards based on IEC 60034-30-1 which is presented in Appendix 1. Asynchronous motors that can be operated only with converters do not have any international efficiency regulations (ABB 2014a), even though IEC is preparing efficiency measurement standards for motors used with converters. Motors in converter use have a lower total efficiency because of the converters supply harmonics which increase additional losses. Even the total efficiency is lower in VSD use with converters than in DOL use, the overall energy consumption is often lower because of the ability to adjust speed according to the load (Kärkkäinen etc. 2017: 45–46).

Total losses of electric motor P_{loss} can be defined as the difference between input power and output power as

$$P_{\text{loss}} = P_{\text{in}} - P_{\text{out}}. \quad (7)$$

The PMSynRM total losses that can be solved with simulations or measurements can be defined as

$$P_{\text{loss}} = P_{\text{Cus}} + P_{\text{Fes}} + P_{\text{Fer}} + P_{\text{fw}}, \quad (8)$$

where P_{Cus} is stator Joule losses, P_{Fes} stator iron losses, P_{Fer} rotor iron losses, P_{fw} mechanical losses. In three-phase PMSynRM the Joule losses which are also called as copper losses or resistive losses are mostly affected in stator windings and can be defined as

$$P_{\text{Cus}} = 3R_s I_s^2, \quad (9)$$

where I_s is stator phase current and R_s stator phase winding resistance. When PMaSynRM is designed only for VSD use, the rotor does not have squirrel cage and the rotor does not create Joule losses as in induction motor.

Stator iron losses P_{Fes} and rotor iron losses P_{Fer} consist of hysteresis and eddy current losses. Iron losses are produced in rotor and stator electric steel sheets by the alternating magnetic flux. Hysteresis losses are in proportion to frequency and depend on the hysteresis loop of the electric steel sheet material. Eddy current losses are in proportion to the square of the frequency. Eddy currents induce easily in large solid objects and can be reduced by using laminated thin electric steel in rotor and stator core. (Piuhola 2003: 14.)

Mechanical losses P_{fw} can be defined as friction losses and windage losses. Friction losses are mostly affected from bearings and they depend on the bearing type, shaft load, used grease, type of shaft sealing and running speed. Windage losses are caused from rotating parts for example from rotor-ends, which may have ventilation blades and balancing material and from the fan installed to the shaft.

In PMaSynRM also some additional losses are generated, also known as stray-load losses which have numerous sources and are caused from different phenomena. In converter-fed motors the additional losses are generated mostly because of the supply harmonics (Kärkkäinen etc. 2017: 45–46). Additional losses measurement methods are defined in IEC 60034-2-1 but it is only for sinusoidal supply and it does not apply for synchronous motors such as PMaSynRM in VSD use. (Hirvelä 2013: 27–28; Pyrhönen etc. 2014: 194–203, 524–534; Söderang 2016: 19.)

2.7 Temperature rise and insulation classes of electric motors

Live parts of electric motor such as winding and power cables, need to be protected against short circuits using insulators. Thermal stresses due to the losses, as well as mechanical and electrical stresses, degrade the properties of insulators. Electric motors are determined with thermal classes based on the used insulation materials. IEC 60085 and IEC 60034-1 standards define the maximum allowed stator winding hotspot temperature for insulation classes, as presented in Figure 8.

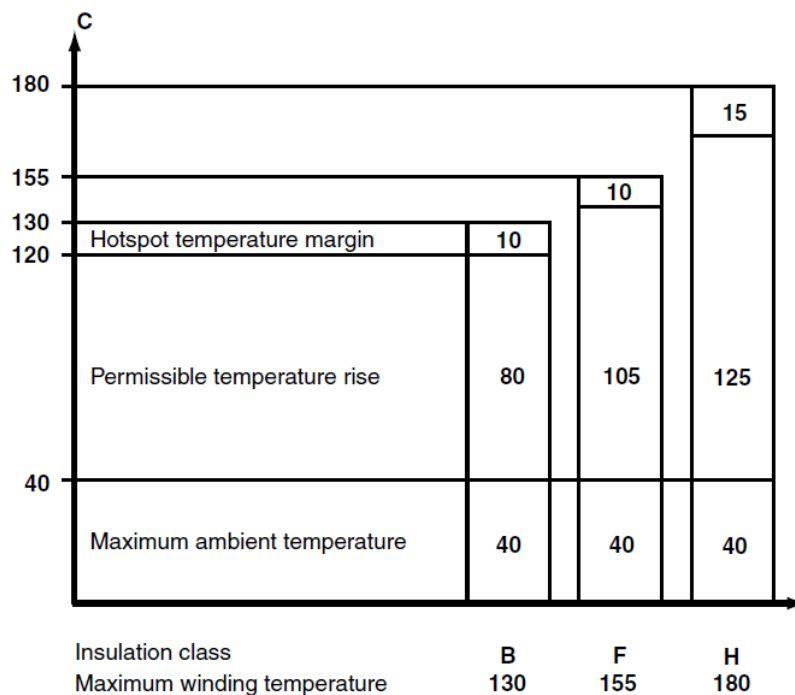


Figure 8. Insulation and thermal classes (ABB 2014b).

Insulation class temperature limit is the winding maximum temperature which is the sum of maximum ambient temperature, permissible temperature rise and hotspot margin which are presented in Figure 8. The permissible temperature rise of motor can be determined by calculating the change of winding resistances, when running a temperature rise test. Winding temperature rise can also be determined by measuring the winding temper-

ature, for example with a thermocouple. When using the last measuring method, the permissible temperature rise is 10 °C higher than with resistance calculation method, which means that class B is 90 °C, class F is 115 °C and for class H is 135 °C.

ABB Motors and Generators in Vaasa uses a 25 °C safety margin in their products, which means that motor designed for temperature rise class B has a class F insulation. Using safety margins in the insulation the life time of insulation is extended and the motor can be overloaded for a short time period (ABB 2014b: 44; Sivunen 2011: 41).

2.8 Effect of temperature to permanent magnet material demagnetization

In PMSynRM it is important to pay attention to the permanent magnet material temperature rise as permanent magnets can be demagnetized. Different permanent magnet materials have different demagnetization properties based to the material's B - H curve. In Figure 9 is normal demagnetization curve where horizontal axis presents reverse direction magnetic field strength H against the permanent magnet flux density B . On horizontal axis there is also presented point of coercivity H_c which presents the point of maximum reverse magnetic field without demagnetization of permanent magnet. The vertical axis shows permanent magnet flux density B with remanence B_r which is the maximum flux density that magnet is able to produce and point of minimum flux density B_k that magnet can withstand without demagnetization. B_k is also called as knee-point. If the reverse direction magnetic field H increases beyond the knee-point, the demagnetization process begins.

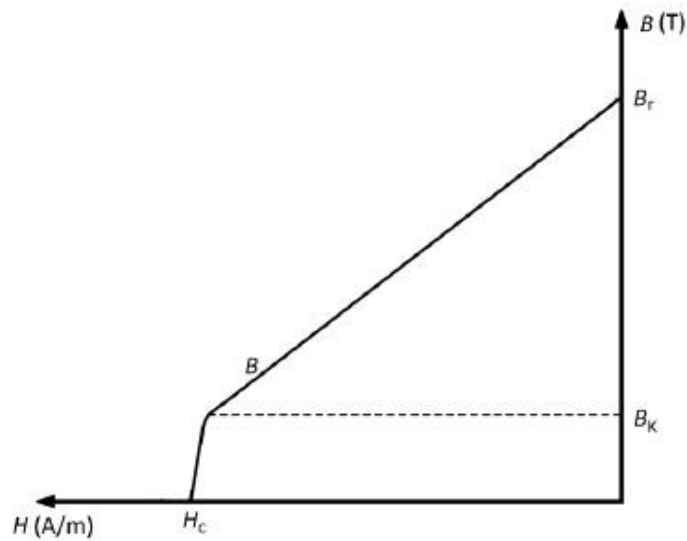


Figure 9. Normal demagnetization curve with remanence B_r , knee-point B_k and coercivity H_c . Modified from (Hirvelä 2013: 20).

From normal demagnetization curves in Figure 10 it can be seen that temperature rise on Samarium Cobalt ($\text{Sm}_2\text{Co}_{17}$) Vacomax 255 HR magnet decreases the magnets remanence B_r , knee-point B_k and coercivity H_c . When comparing different permanent magnets demagnetization properties as Vacomax 225 HR in Figure 10 and Neorem 595a in Figure 11, it can be noted that Vacomax 225 HR can withstand much higher temperatures in equal strength reverse magnetic field H without demagnetizing. In this thesis' PMSynRM development project Vacomax 225 HR permanent magnets are used.

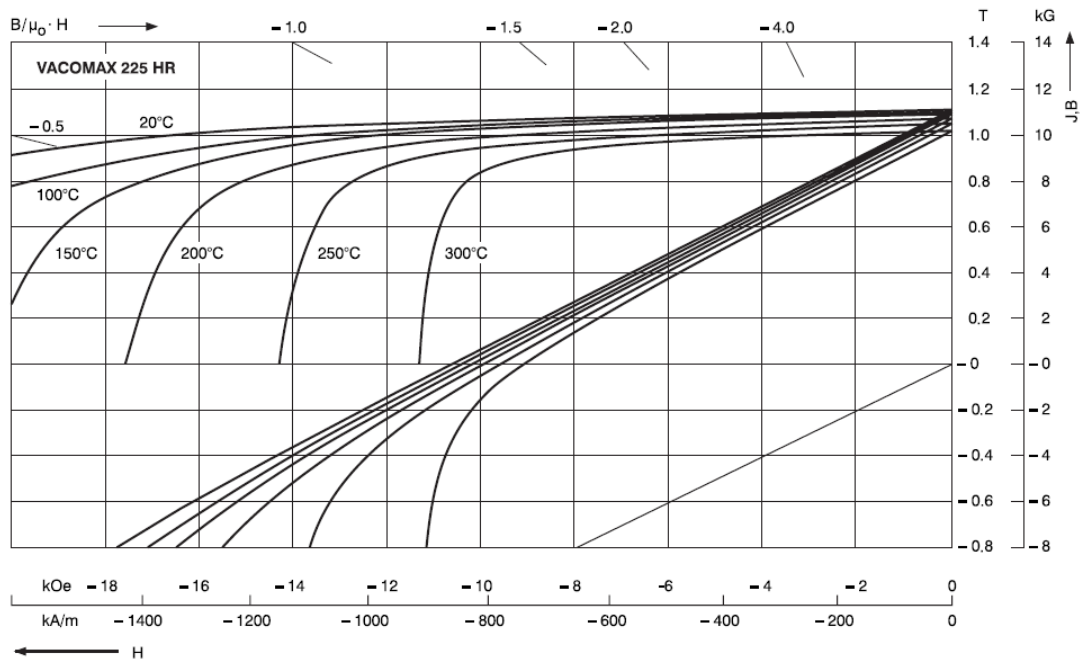


Figure 10. Typical demagnetization curves of Sm₂Co₁₇ Vacomax 225 HR magnet at different temperatures (VAC 2014: 45).

For an alternative magnet material comparison in Figure 11, the demagnetization curves of Neodymium Iron Boron (NdFeB) Neorem 595a magnet is presented.

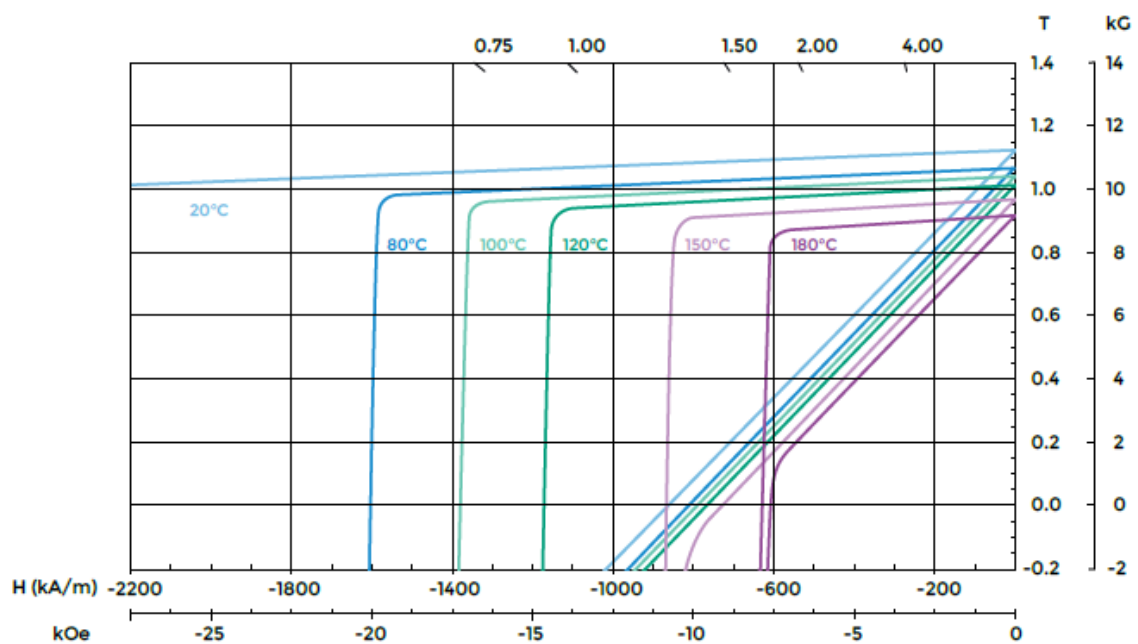


Figure 11. Typical demagnetization curves of NdFeB Neorem 595a magnet at different temperatures (Neorem Magnets 2014).

3 ABB HIGH DYNAMIC PERFORMANCE SERIES MOTORS

ABB Motors and Generators' high dynamic performance series motors are induction motors in IEC frame sizes 100–250. The HDP motor design does not have a separate outer frame with cooling ribs, only a stator core which has square shape on the outside. The HDP series motors have an open design with two different degree of ingress protection (IP), which are IP23 and IP54 according to IEC 60034-5 standard. The HDP series rotors are squirrel cage rotors manufactured from die-cast aluminum or copper bars, depending on the frame size and protection class. The HDP series motors are designed only for VSD use and the motors are equipped with external cooling fan units. In the HDP series cooling method is used forced convection based on IEC 60034-6. The IP54 version is equipped with axial cooling fan motor and IP23 with radial cooling fan motor. Forced convection transfers the heat out from the stator core, through the stator core ventilation ducts which are presented in Figure 12. In the HDP series motors some forced convection air flows also through the air gap between stator and rotor, but it has minimal cooling effects. The outer surface of stator does not have any cooling ribs and heat transfer of the outer surfaces is minimal, based on natural convection and a very limited conduction from the motor mounting surfaces.

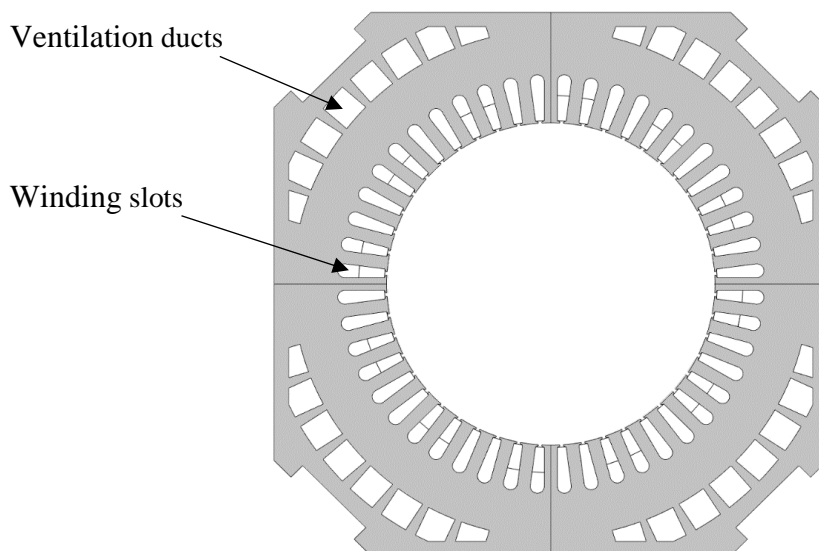


Figure 12. Two-dimension drawing of HDP 250 stator with ventilation ducts and winding slots.

In Figure 12, where a two-dimension drawing of HDP square stator sheet is presented can be also noted the stator winding slots. When the stator electric steel sheets are stacked together they structures the stator core.

In this thesis, a PMSynRM prototype rotor is designed to match a 250 frame size HDP stator with IP23 protection. The basic structure of IP23 protection class HDP series motor is presented in Figure 13.

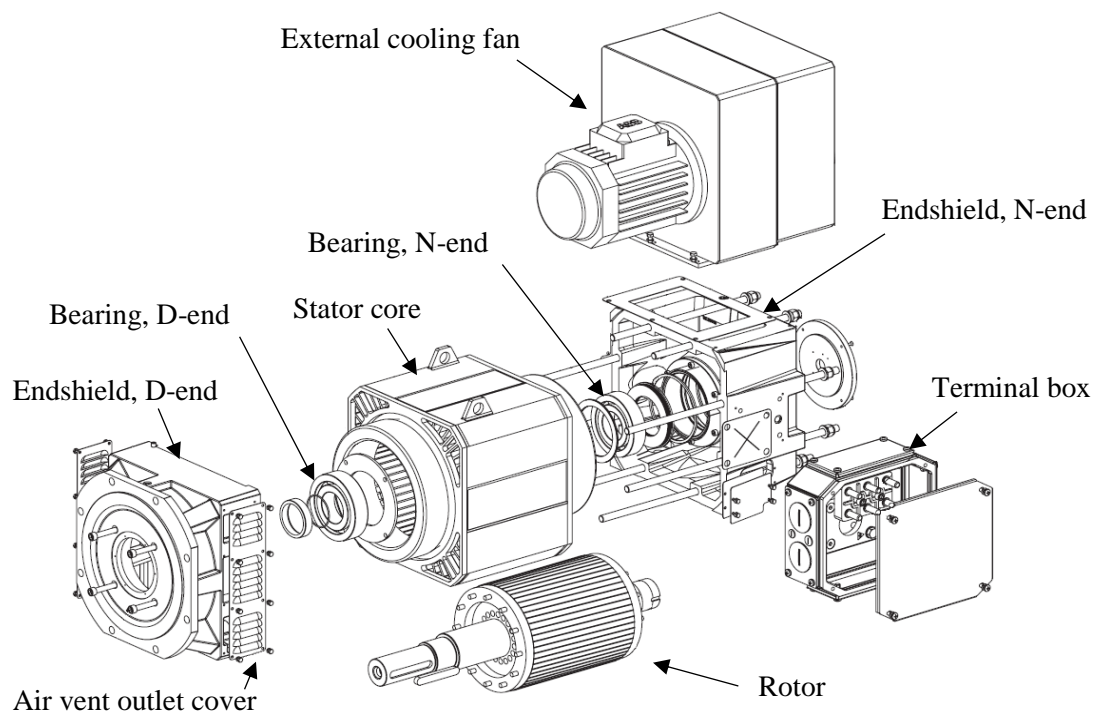




Figure 13. Drawing of IP23 protection class HDP series motor with external radial cooling fan unit. Modified from (ABB 2015a: 59).

The IP23 protection class HDP series motor's most common parts are stator frame which is also the motor body and endshields in drive end (D-end) and in non-drive end (N-end) of the frame. Rotor with shaft and bearings in both ends, terminal box, cooling fan unit and air vent outlet cover as presented in Figure 13 are the most common parts. HDP series motors manufactured by ABB Motors and Generators in Vaasa has small size and a light weight compared to same output power level enclosed Process Performance induction motors. A comparison of the two different induction motor types is presented in Table 2.

Table 2. Comparing ABB's High Dynamic Performance series and Process Performance series motors when temperature rise class is F and output power 560 kW (ABB 2014c: 22; ABB 2015a: 50).

	M3EH 250E 4	M3BP 355LKB 4
Figure		
Product code	3GEH252754-•DA	3GBP352820-••G
IEC frame size	250	355
Power output (kW)	560	560
Weight (kg)	1423	2600
Inertia (kgm ²)	4.12	10.6
Ingress protection (IPXX)	IP23	IP55
Voltage (V)	400	400
Temperature rise class	F	F

Motor type M3EH 250E 4 in the Table 2 describes a catalogue HDP series motor and the motor type M3BP 355LKB 4 describes a conventional enclosed process performance motor. Both motors are induction motors with output power 560 kW. From Table 2 it can be noted that the HDP series motor has extremely low weight compared to the enclosed motor with same output level, which means that HDP series motor has a higher power density. The low weight of HDP series motor results in also a low inertia. HDP series motors are ideal for industry application where high output power and a low moment of inertia is needed but where also the motor size or weight is a limiting factor. HDP series motors are ideal to replace DC motors for example in plastic and rubber extruders, paper printing machines and metal presses. They are also ideal for automotive test stands. (ABB 2015a: 5, 51; ABB 2014c: 22; Pyrhönen etc. 373–376, 534.)

4 PROTOTYPE DESIGN OF PMASYNRM

Electric motors are used in countless applications and environments which set several requirements in mechanical and electrical properties. Finding an optimal electric motor for a specific application is not always easy or even possible at all, which leads on a question if it is possible to design. Nowadays electric motor designers' most important everyday tool is a calculation software that can solve motors equivalent circuit from given parameters. Motor designing can be also done in traditional way, manually, but it takes much time, due to the change of varying impedance values and several iteration cycles (Talvitie 2005: 13).

There are several methods to design electric motors of which one is to modify an existing catalogue motor. The modification of catalogue motor can be focused in improvements either on electrical, mechanical or on both properties. The electrical modification can be for example a stator windings modification for a specific running speed or a complete motor type change, which can be carried out with a different type of rotor (Kolehmainen 2012a: 2). When the modification or a new design is completely optimized and analysed a prototype can be built to verify the motor's real properties (Kolehmainen 2011: 27).

Manufacturing processes of prototype may need to have some compromises when compared to a larger series of commercial motors. However, it is recommendable to design the motor so that it is simple and low cost to manufacture also in large series. When designing prototype, the used materials and manufacturing methods should be considered from an environmental-friendly view. Life-cycle assessment based to ISO 14040 and ISO 14044 standards is one of the methods to investigate these questions and the eco-design requirements set by European Union Directive 2009/125/EC, Commission Regulation 640/2009.

4.1 Design method of PMaSynRM

In this thesis, a standard IEC 250 frame size HDP series motor's electrical properties are modified with a change of induction rotor to a PMaSynRM rotor. The aim is to design a HDP 250 PMaSynRM to reach better electrical properties and thermal behaviour. A new PMaSynRM rotor is designed but the HDP series stator is kept as standard. The PMaSynRM prototype rotor design procedure is presented in Figure 14, which begins from guess of starting parameters that bases on designer's experience. Next step is to optimize the motor by determining the rotor parameters. The success of optimization can be inspected by analysing the simulation results with Finite Element Method (FEM). The guessed starting parameters and rotor optimization parameters are refined if the goal has not been reached. When the goal is reached based to the FEM analysis results, a prototype rotor can be manufactured and tested to verify the results of FEM analysis (Khan 2012: 9, 19, 41; Kolehmainen 2011: 27, 28).

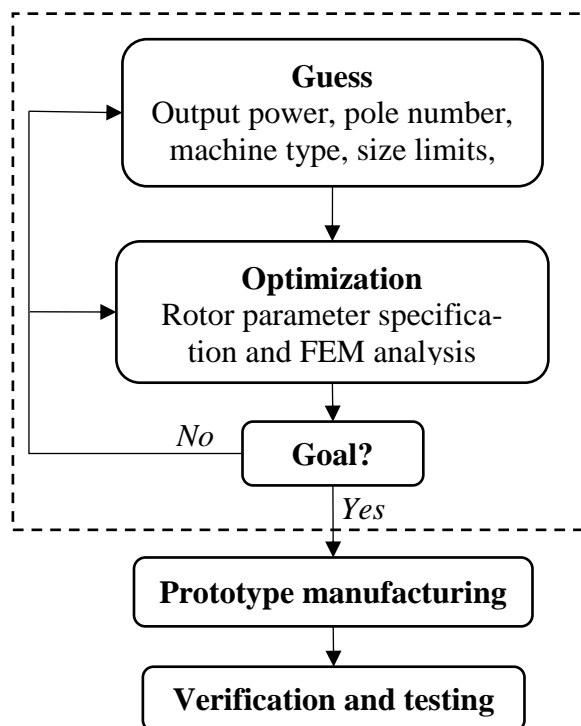


Figure 14. Flow chart of prototype rotor designing.

Guess

First the guess of basic parameters is done for output power, number of phases, number of poles, rated torque, rated speed, stator inner diameter and total axial length as presented in Figure 14 (Khan 2012: 9–13). The guessed initial parameter of HDP 250 PMSynRM used in this thesis are:

- Three phases and four poles
- Output power 600 kW
- Constant torque area 525–1050 rpm
- Constant power area 1050–3000 rpm
- Field weakening point 2400 rpm
- Maximum speed 3000 rpm
- Voltage 400 V
- Stator inner diameter 295.0 mm
- Total axial length 660 mm.

The mechanical dimensions of PMSynRM rotor is kept the same as HDP series induction rotor, within the limits of stator inner dimension which allows changes of the air gap length.

Optimization and Goals

The goals of PMSynRM can be presented with single performance values for example nominal current, power factor and efficiency. The single performance values are dependent from each other, which leads on a situation that all the values cannot be the best at the same time. To design an electric motor for a high overall performance, it is needed to make compromises compared to a single performance value in optimization. Performance values can be weighted for example based to the application, duty class type and supply network limitations and requirements. When designing a motor for high overall performance, a multiple criteria optimization is needed. Multiple criteria optimization generates set of an equal solutions which are also called as Pareto optimal solutions. Typical for

Pareto optimal solution is that one single performance value cannot be increased anymore without decreasing the other performance values (Ryyppö 2005: 11–13).

The Pareto optimal front performance values used for HDP 250 PMSynRM are:

- maximized output power (kW)
- maximized nominal efficiency (%)
- maximized nominal torque (Nm)
- maximized power factor
- minimized nominal current (A).

After the rotor's electrical properties are optimized, the stator windings can be modified depending on the motor running speed (Kolehmainen 2012a: 2).

4.2 Rotor parametrization of PMSynRM

In this PMSynRM prototype development project only the rotor is designed and optimized. PMSynRM rotor optimization bases on designing rotor magnetic properties to create a compatible magnetic circuit with stator. The rotor core optimization includes designing of rotor electric steel sheet, magnet placements and magnet material. The rotor electric steel sheet optimization considers number of flux barriers, flux barrier geometrical parameters, magnet slots, insulation ratio and flux barrier dimension along the d -axis and q -axis (Khan 2012: 9–13; Hirvelä 2013: 45–55). The rotor mechanical properties are also optimized and analysed so that rotor is robust for determined running speeds (Kolehmainen: 2011: 28).

Geometry and number of flux barriers

Number of flux barriers has effects on the flux distribution through in the rotor and on the average torque production. Rotor flux distribution can be evened out by using multiple number of flux barriers and average torque can be increased when the number of flux

barriers are increased up to four or five. Greater number of flux barriers has not found given increasing effect on average torque. Increasing number of flux barriers reduces torque ripple, decreases harmonic losses and decreases demagnetisation risk (Khan 2011: 10–11; Luo, Zhao, Ji, Zheng, Zhang, Ling, Mao 2017: 1). The rotor geometry of this PMaSynRM prototype is modified from an earlier designed rotor with a result of four flux barriers per pole as presented in Appendix 2. The rotor sheets are chosen to be made of Grade EN 10106 cold rolled non-oriented M350-50A electric steel. The thickness of the electric steel is 0.50 mm and the relative permeability at 1.5 T is 1020. When designing flux barriers, it should be taken under consideration what is the shapes and sizes of PM materials available on markets because the PM material is assembled in the flux barrier.

Permanent magnet material and placement

The permanent magnet material is chosen to be Sm₂Co₁₇ Vacomax 225HR which has high demagnetization and heat tolerance up to 350 °Celsius. At 20 °C temperature the magnet material remanence B_r is 1.1 T and the coercivity H_c is 820 kA/m. The temperature coefficient of remanence α is -0.030 %/°C (VAC 2014: 18–19). Temperature rise in permanent magnets is factor for the demagnetization. The temperature rise in PMs can be estimated with the assumption of dependency between remanence B_r and induced open circuit voltage U_{oc} , which is linear. The temperature rise in PMs can be estimated as

$$\Delta T_{PM} = \frac{B_{r,20^\circ C}}{\alpha U_{oc,20^\circ C}} (U_G - U_{oc,20^\circ C}), \quad (10)$$

where $B_{r,20^\circ C}$ is remanence and $U_{oc,20^\circ C}$ induced open circuit voltage at 20 °C temperature (Hirvelä 2013: 43–44). The demagnetization curve of Vacomax 225HR is presented in Figure 10.

The magnets placements can be designed with lots of different ways as presented in Figure 15 where magnets are on the d-axis (a), on both axes (b), only on q-axis (c) and (d)

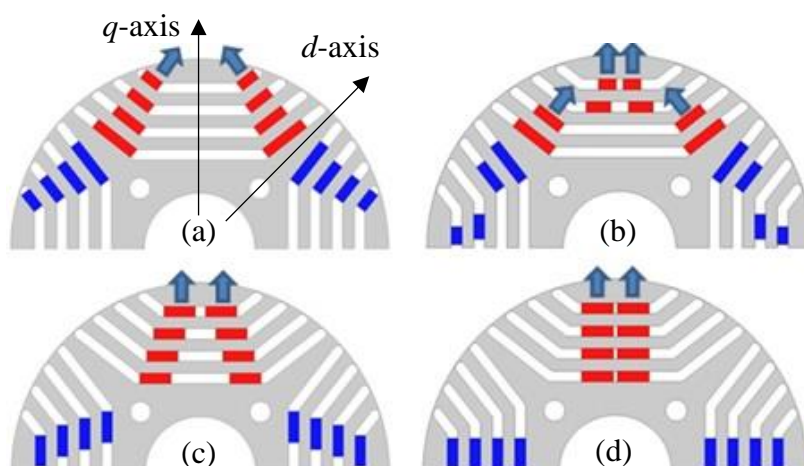


Figure 15. Different permanent magnet material placement types in 4-pole rotor sheets where magnets are on the d-axis (a), on both axes (b), only on the q-axis (c) and (d). Modified from (Liu, Kim, Oh, Lee, Go 2017: 2).

The two-dimension drawing of rotor in Figure 16 presents one quarter of the designed PMaSynRM's four-pole rotor, where the magnet placements coloured with yellow can be seen.

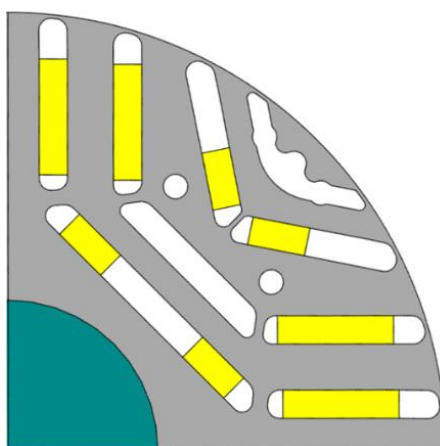


Figure 16. Magnet placement of the designed PMaSynRM prototype rotor.

The magnet placements are designed on both flux barriers axes-directions and some of the flux barriers is left empty as can be seen from Figure 16. The empty flux barriers can be exploited in future, if one wants to study a rotor with higher volume of magnets.

Mechanical stresses

The rotors mechanical properties are analyzed with Comsol Multiphysics® at 3600 rpm and results are presented in Figure 17. The maximum von Mises stresses are 200 MPa which allows for maximum rotating speed of 3660 rpm.

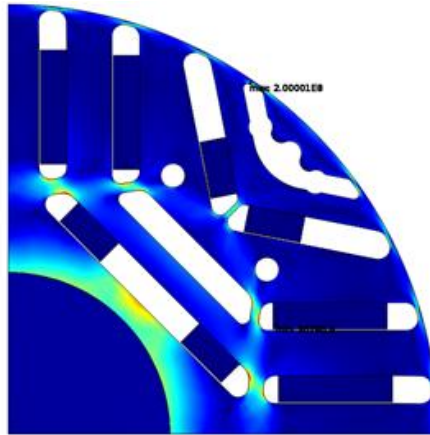


Figure 17. Maximum mechanical stresses simulated with Comsol Multiphysics®

The HDP 250 PMaSynRM prototype design specifications are:

- Rotor outer diameter 292.6 mm
- Total axial length 660.0 mm
- Air gap length 1.2 mm
- Four flux barriers per pole
- Permanent magnet material $\text{Sm}_2\text{Co}_{17}$
- Permanent magnet material length 60.0 mm, width 19.4 mm and depth 9.0 mm
- Totally 528 pcs of magnets inside the rotor.

The length of $\text{Sm}_2\text{Co}_{17}$ magnet is 60.0 mm and the total length of rotor core is 660.0 mm. In the magnet slots of rotor core, number of 11 magnets can be assembled in a row to meet the full length of magnet slot. From each pole of the rotor is used 12 magnet slots for magnet assembly as presented in Figure 16. As the rotor is designed with four poles and from each pole is used 12 magnet slots and in each magnet slot is assembled 11 magnets, the total number of assembled magnets is $4 \cdot 12 \cdot 11$ which totals 528 pieces.

5 SIMULATION RESULTS USING ADEPT FCSMEK

In this chapter the Adept FCSmek simulation results of PMSynRM are presented. The motor is designed for VSD use and the simulations are performed for a wide constant power speed range. The motor operating points are solved with the calculation method to find the motor voltage with the lowest current. Reason that the motor is designed according to voltage with lowest current is because the converter sizing depends on the current and power factor. It is also stated that the optimal voltage with the lowest current nearly achieves the highest efficiency (Hirvelä 2013: 31, 57).

The PMSynRM motor is first simulated with Adept FCSmek time harmonic solver in DOL use with sinusoidal line voltage. The time harmonic solver has a short calculation time but the results have some shortcomings for example in iron losses (Talvitie 2005: 53). The voltage for lowest current is solved for output levels 150–600 kW with line frequency at 17.5–100 Hz which is 525–3000 rpm. When voltage with the lowest current is found, the FCSmek time stepping calculation is done for more accurate results. The time stepping method takes a long calculation time because of many iteration cycles but it is able to model iron losses, which depend on the harmonics and non-sinusoidal magnetic flux (Talvitie 2005: 41). As the prototype of PMSynRM is designed for VSD use, the time stepping calculations are also done with line voltage setting: Simple 2-level DTC.

PMSynRM rotor and IM aluminium squirrel cage rotor are modelled and compared in the same HDP 250 stator design. Although the designed PMSynRM can be used only with converter, the calculations are done with DTC and DOL for more comprehensive comparison to the induction rotor. The aluminium squirrel cage induction rotor has been designed and tested before this PMSynRM prototype project, so the calculation results of IM are done by exploiting the measurement results. IM is calculated with 500 kW and with 575 kW which is the highest output power that could be tested because of high temperature rise.

PMSynRM and IM calculations are done with 60 Hz line frequency. PMSynRM simulation is done with 500 kW output for equal comparison for the IM and with 600 kW

output regarding to the designing goal of output power. Friction losses in both motors are decided to be 0.285 kW when using 60 Hz line frequency. Adept FCSmek FEM simulation results are presented in Table 3 where U_{mot} is the motor supply voltages fundamental waveform only.

Table 3. Adept FCSmek simulated FEM results of 3-phase and 4-pole PMaSynRM and induction motor in DOL and DTC use at 60 Hz line frequency which corresponds to running speed 1800 rpm.

Type and connection	P_{out} (kW)	T (Nm)	η (%)	U_{mot} (V)	I (A)	$\cos\phi$	P_{Cus} (kW)	P_{Fes} (kW)	P_{Cur} (kW)	P_{Fer} (kW)	P_{loss} (kW)
PMaSynRM DOL	500	2653	97.76	437	786.8	0.86	4.94	4.99	-	1.25	11.48
PMaSynRM DOL	600	3183	97.73	456	920.3	0.85	6.76	5.44	-	1.44	13.92
PMaSynRM DTC	500	2653	97.37	440	799.6	0.84	5.14	5.82	-	2.46	13.70
PMaSynRM DTC	600	3183	97.37	461	935.3	0.84	7.04	6.33	-	2.78	16.42
IM DOL	500	2653	96.60	400	847.1	0.88	5.58	4.34	6.45	0.96	17.62
IM DOL	575	3183	96.35	400	964.1	0.89	7.21	4.59	8.64	1.07	21.80
IM DTC	500	2653	96.06	402	825.8	0.91	5.79	4.86	8.11	1.44	20.48
IM DTC	575	3183	95.87	403	941.7	0.92	7.38	5.20	10.46	1.53	24.86

From Table 3 simulation results we can see that PMaSynRM does not produce any rotor Joule losses, which can be seen as a result of PMaSynRM's lower total losses and higher efficiency when compared to IM with same output power. From Table 3 can be also noted that in PMaSynRM and IM, the DTC use increases loss production and decreases efficiency when compared to DOL use.

5.1 Current and power factor of PMaSynRM and IM

Converter sizing depends on current and power factor. Current is also a limiting factor when sizing the power cables. Figure 18 presents the simulated current and power factor of PMaSynRM and IM in DOL and DTC use at 500 kW output level with 60Hz supply frequency.

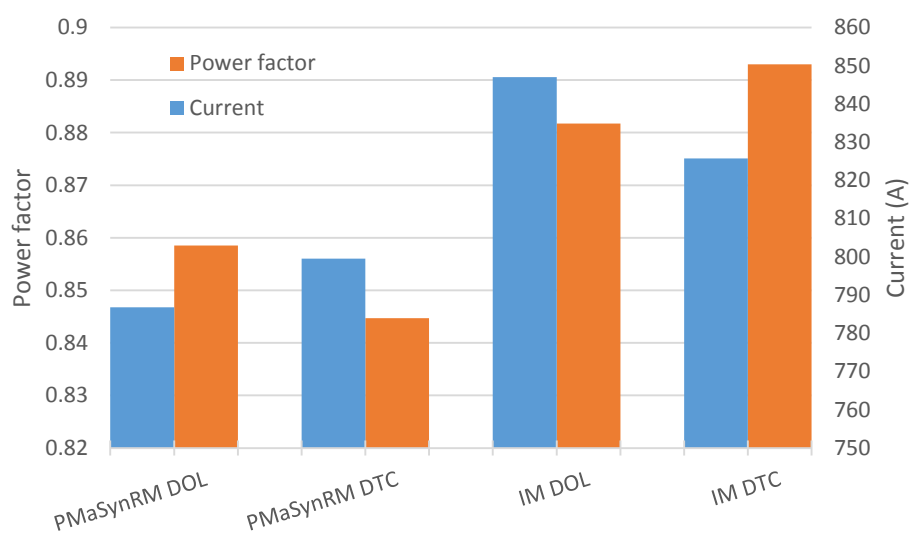


Figure 18. Current and power factor of PMaSynRM and IM with DOL and DTC use at 500 kW output with 60 Hz supply frequency.

From the simulation results of current and power can be noted that PMaSynRM has lower current but also a lower power factor than IM. In PMaSynRM the current increases and the power factor decreases in DTC use as in IM the current decreases and power factor increase in DTC use. The PMaSynRM simulation results are in the line with expectations but the IM simulation results behave differently.

5.2 Losses and efficiency of PMaSynRM and IM

PMaSynRM is simulated with 500 kW and 600 kW output levels and IM is simulated with 500 kW and 575 kW output levels. Simulated losses with Adept FCSmek in DOL

sinusoidal supply is presented in Figure 19 where total losses are divided to partial losses. Mechanical losses at 60 Hz, which corresponds to speed 1800 rpm, are 0.285 kW in all cases.

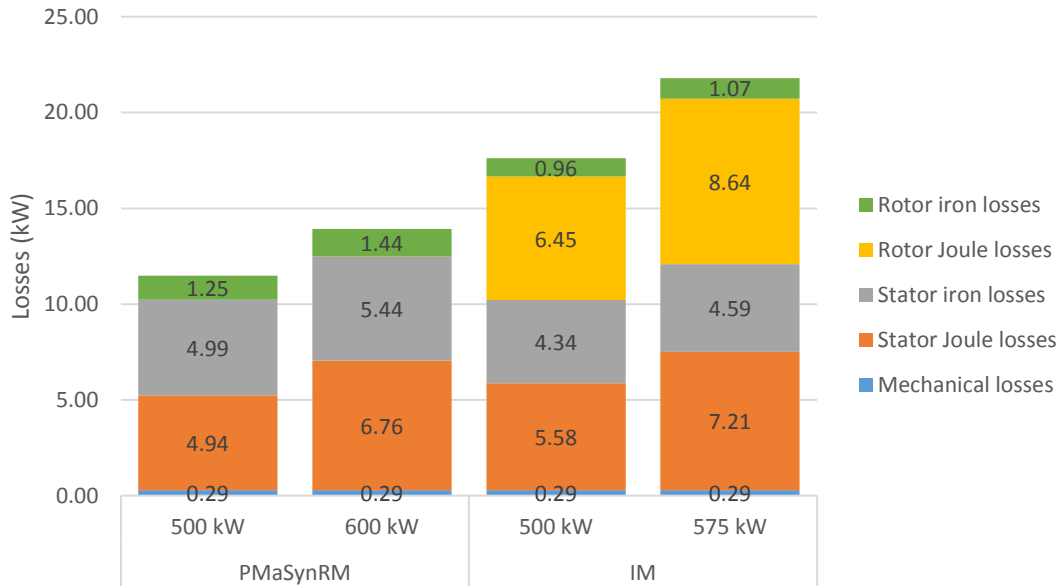


Figure 19. Calculated PMSynRM and IM partial losses at different output power with 60 Hz sinusoidal DOL supply.

From Figure 19 it can be seen that stator Joule losses are a bit higher in IM when comparing to same output level of PMSynRM. Instead in PMSynRM the stator iron losses and rotor iron losses are a bit higher than in IM. Rotor Joule losses are the major losses in IM which increases the total losses of IM while PMSynRM does not have any rotor Joule losses. With 500 kW output power the IM total losses are 53.5 % higher than the PMSynRM total losses. IM at 500 kW output level has higher total losses even when compared to PMSynRM at 600 kW output level.

Figure 20 presents the difference in loss production when the sinusoidal DOL supply is changed to DTC supply.

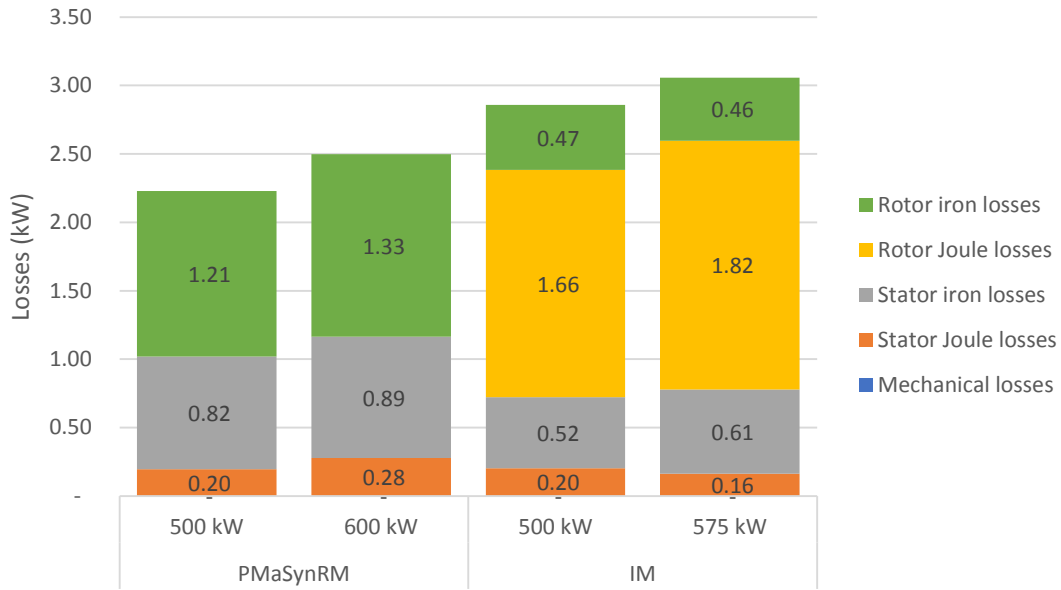


Figure 20. Increase in PMSynRM and IM partial losses with 60 Hz DTC supply compared to DOL supply with 60 Hz shown in Figure 19.

From Figure 20 it can be seen that excluding mechanical losses all the PMSynRM and IM partial losses at all output power levels increase with DTC supply compared to sinusoidal DOL supply. PMSynRM rotor iron losses with DTC supply increases 96.7 % at 500 kW output power level and 92.6 % at 600 kW output power level when compared to the DOL supply. IM rotor iron losses with DTC supply increases 49.2 % at 500 kW output power level and 42.8 % at 575 kW output power level when compared to DOL supply. DTC supply has also strong effect on the rotor Joule losses in IM, which increases 25.8 % at 500 kW output power level and 21.0 % at 575 kW output power level when compared to DOL supply. In DTC use the rotor and stator iron losses increase more in PMSynRM than in IM when comparing to the same output power level of 500 kW. The stator Joule losses increase is minimal in both motor types with DTC use.

The sum of partial losses is directly proportional to the efficiency of electric motor as it is presented in Equations 6, 7 and 8. Figure 21 presents the simulated efficiencies of PMSynRM and induction motor with sinusoidal DOL and DTC at 60 Hz supply frequency.

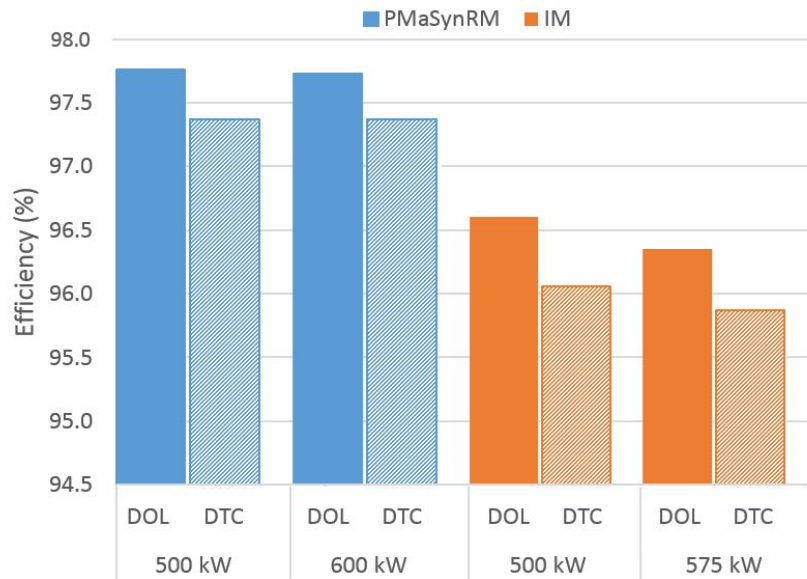


Figure 21. PMSynRM and IM efficiencies calculated with Adept FCSmek in two different output levels with 60 Hz supply frequency in DOL and DTC use.

From Figure 21 it can be clearly noted that DTC use affects lower motor efficiency in both motor types and at all output power levels compared to DOL use, because VSD use increase losses. PMSynRM efficiency at 500 kW output power in DTC use decrease 0.39 percentage points and at 600 kW output power 0.36 percentage points compared to DOL use. IM efficiency at 500 kW output power in DTC use decrease 0.54 percentage points and at 575 kW output power 0.48 percentage points compared to DOL use. It can be also noted that PMSynRM has an overall higher efficiency in all output power levels than IM. Higher efficiency of PMSynRM is mostly affected from the lack of rotor Joule losses as can be seen from Table 3.

Efficiency of PMSynRM in DOL and DTC use stays more balanced with the function of output power than the efficiency of IM. The PMSynRM efficiency in DOL use with 500 kW output power is 97.76 % and at 600 kW output power 97.73 %, which means that the efficiency decreases only 0.03 percentage points for 100 kW output power rise. PMSynRM efficiency in DTC use at 500 kW and 600 kW output power stays on the same level which is 97.37 %.

The IM efficiency in DOL and DTC use decrease effectively with the function of output power as the IM efficiency in DOL use at 500 kW is 96.60 % and at 575 kW it is 96.35 %, which means 0.25 percentage points decrease for 75 kW output power rise. In DTC use the IM efficiency is at 500 kW output power 96.06 % and at 575 kW output power it is 95.87 %, which means 0.19 percentage points decrease for 75 kW output power rise.

6 MANUFACTURING PROSESS OF PMASYNRM PROTOTYPE

Prototype building has an important role because it shows the real performance and characteristic of the designed product. Prototype testing also acts as a measuring instrument for the designing methods and FEM simulation programs when the measured values is compared to the calculated values. Prototype manufacturing process, methods and materials high quality is needed to give a great importance, so that the manufactured product accords what has been designed.

As also in earlier chapters it was mentioned that in this thesis a standard HDP series catalogue motor is modified to a PMASynRM, with the method where only a new rotor is designed. In this chapter, the PMASynRM rotor is first manufactured based to the designed specifications, after which the motor is assembled. This chapter bases mostly on a practical view of manufacturing a prototype of PMASynRM. The aim of this chapter is to introduce prototype manufacturing process and methods, and to bring up the questions that was faced during the manufacturing process.

The PMASynRM rotor consist from several different components which are for example rotor shaft, rotor electric steel sheets, permanent magnet material, endplates, rotor cooling wings, stud bolts, hexagon nuts, washers and two component epoxy glue. Rotor manufacturing includes that some of the components is needed to be manufactured and some of them are standard components which can be find from a hardware store. When all the components are ready, the rotor can be assembled. When the rotor is assembled and balanced the rotor can be assembled inside the stator which needs some special tools because of the rotor magnetic forces.

The PMASynRM prototype manufacturing process can be divided in several parts which are presented in Figure 22 which consist first from rotor sheet manufacturing and rotor endplates and cooling wings manufacturing. PMASynRM manufacturing also needs some special assembly tools which are explained below. The assembly process can be divided in rotor sheet stacking, shaft assembly to rotor core and permanent magnet assembly. Finally the rotor is balanced and assembled to the motor.

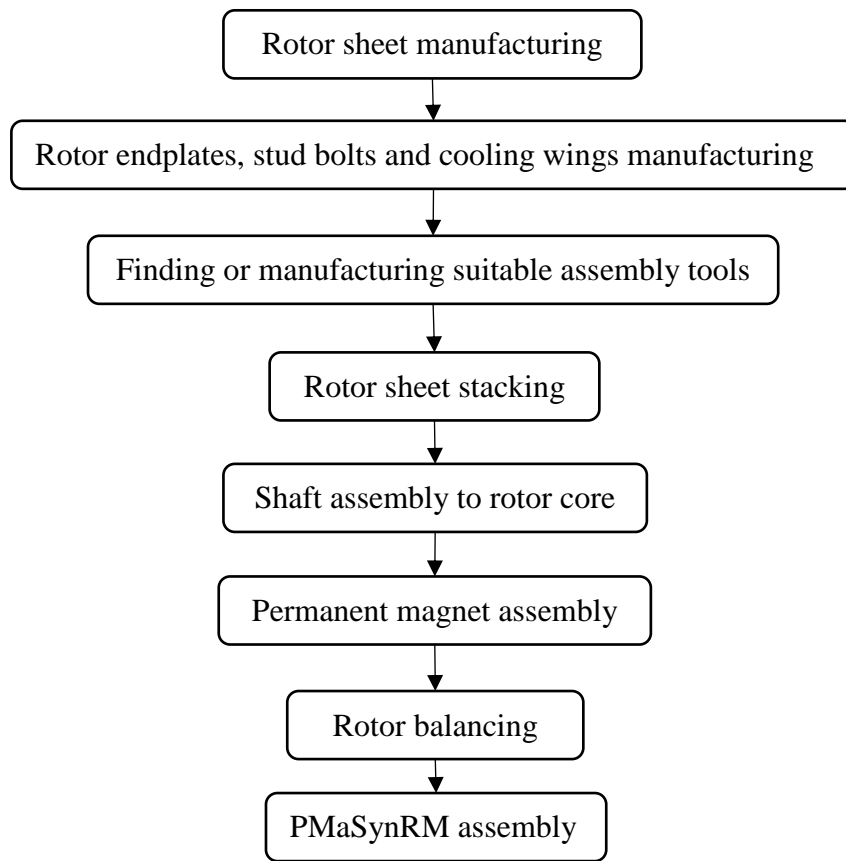


Figure 22. PMA SynRM prototype rotor manufacturing procedure.

6.1 Rotor electric steel sheet and rotor endplates manufacturing

Rotor electric steel sheet manufacturing bases on the designed structure which has reached the goal after analytical and FEM designing cycles. Rotor electric steel sheets, as well as stator electric steel sheets, have two ways to be manufactured to the desired shape. One method is mechanical punching and another is laser-cutting. Alternative manufacturing methods have effects on the steel sheets electrical, magnetic, mechanical and thermal behavior. Mechanical punching is a conventional way to process the electric steel sheets especially when produced in larger series. Laser cutting is used especially when manufacturing smaller series of electric steel sheets, for example in prototype building. Laser cutting has been claimed to increase iron losses and to reduce magnetic properties of the material. Laser cutting may also leave some burrs on the slot edges depending on the cutting techniques (Bali & Muetze 2014: 1443; Moghaddam 2011: 212).

In this PMaSynRM development project the rotor electric steel sheet material is M350-50A non-oriented laminated electric steel. The manufacturing method is chosen to be laser cutting because there is no suitable punching tool available and it is not reasonable to manufacture a new punching tool only for the prototype. To ensure sufficient quality for the rotor electric steel sheets, a random check was made by picking up rotor sheets randomly from a pile of ready rotor sheets to find out the slot edges smoothness. If there is left some burrs or thresholds, there may be later a problem in the magnets assembly because the magnets may be stuck against the burrs. Also, the rotor core may become asymmetric if the steels sheets have different thickness due the burrs. Figure 23 presents one of the laser-cut rotor electric steel sheets.

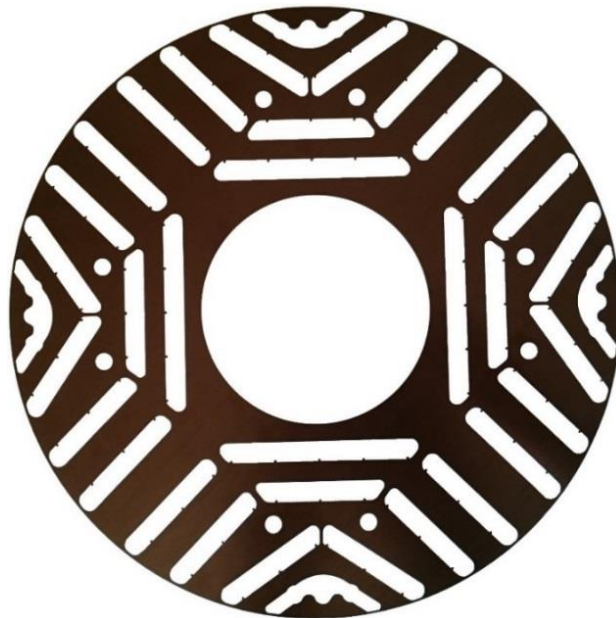


Figure 23. PMaSynRM prototype rotor's electric steel sheet manufactured by laser cutting.

Rotor endplates are designed to hold up the pressed rotor core with stud bolts. Endplates equalizes the pressure of the stud bolts evenly to the whole rotor sheet area. They also enable of fixing cooling wings and balancing screws. The endplates are manufactured from austenitic stainless steel material, to prevent flux leakage, because it has low permeability as is presented in Appendix 3. The stainless-steel endplates are manufactured with laser cutting and the threads are machined. The quality of endplates is inspected by

checking all the machined threads and openings to avoid any problems in later steps of assembly. Figure 24 presents the back endplate with attached stud bolts.



Figure 24. Stud bolts fixed in the rotor back endplate's threads.

6.2 Rotor core assembly

Rotor core consist from a numerous electric steel sheets stacked together. In this prototype building project, the electric steel sheets are stacked together between the rotor endplates and fixed with stud bolts made of stainless steel. The first step in rotor core assembly is to fix the threaded stud bolts tightly to the back endplate threads as is presented in Figure 24. Next the endplate with tightened stud bolts is set to the assembly stand which has a bit smaller diameter assembly post than the diameter of the shaft. The rotor electric steel sheets are stacked in piles through the assembly post and stud bolts as is shown in Figure 25.



Figure 25. Rotor electric steel sheets are stacked in piles through the assembly post and stud bolts.

When stacking the rotor sheets, it should be checked that no slices is left inside the slots so that every laser cut slot is open. After it is checked that all the rotor sheets are good enough, the sheets can be stacked in piles. The piles are stacked so that every other pile of rotor steel sheets is turned in 90 degrees from each other's based on the steel sheets rolling direction. The Reason that the piles are stacked in 90-degree turns is aiming to manufacture a magnetically asymmetrical rotor (Shin, Kim, Lee, Lim, Wiedenbrug 2015: 2896).

The rotor electric steel sheet rolling direction can be manually checked from the direction of steel sheet lamination stripes as presented with double-ended arrow in Figure 26.

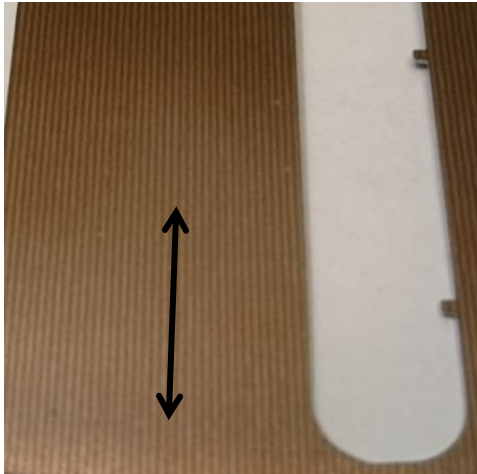


Figure 26. Laminated surface of rotor electric steel sheet where the lamination stripes presents the steel sheet rolling direction.

Rotor sheets are piled as many as rotor core meets the designed length. The length is measured from the compacted rotor core. The rotor front endplate on the top of the rotor core is needed to avoid any rotor sheet damages when pressing the core as is presented in Figure 27.



Figure 27. Stacked rotor core with rotor front endplate after pressing.

When the pre-determined rotor length is reached the endplate will be fixed tightly to the core with stud bolts and hexagonal nuts. There is a need to use correct tightening torque when tightening the endplate with hexagonal nuts to avoid damaging the stud bolts threads. Tightening torques for metric fasteners bases on ISO 898 standard which defines the torque related to the material strength class and material size.

6.3 Shaft assembly in to the rotor core

In this prototype building project, the shaft diameter of rotor sheets are designed to be a bit smaller than the shaft which affects that the shaft is needed to be installed by pressing or by using heat expansion. In this prototype project it was decided to use heat expansion method by heating the rotor core in oven, after which the shaft is installed. When the rotor core has reached the desired temperature it is taken out from the oven and the shaft is let down through the rotor core with its own weight. The shaft needs to be marked in the correct position in relation to the rotor core. When the shaft is set on its correct position it is needed to be waited that the rotor core cools down and the shaft heats up, so the clearance between two components decreases and stick together making a tight connection. Figure 28 presents the rotor core with shaft after the shaft assembly, where can be also noted that the rotor core has changed colour because of high temperature.



Figure 28. Rotor core with installed shaft.

Straightness of rotor shaft and rotor core is important to verify because rotor is needed to be in a center position in relation to the stator. The shaft and rotor core straightness can be checked when the rotor is cooled down to the ambient temperature.

One method in rotor designing and manufacturing is to design the rotor sheets diameter to oversize, so that rotor core straightness can be ensured by machining the outer surface which also smoothens the outer surface. In this prototype manufacturing project, the rotor sheets are designed and laser cut to the determined size, which affects that the outer surfaces cannot be machined. However, the straightness measurements of this prototype's shaft and core proves to be inside the manufacturing tolerances (ABB 2012).

6.4 Rotor magnet assembly

There are two different options in the magnets assembly process where one is to assemble the magnets first inside the rotor which after the rotor is balanced, before installing rotor in to the stator. Advantages of installing magnets first is that the rotor can be balanced with magnets. The disadvantages are that rotor installation inside the stator is challenging because of rotor's magnetic forces. Another way to assemble the magnets is that the rotor is first balanced without magnets, which after the rotor is installed inside the stator and at last the magnets are assembled inside the rotor. Advantages of installing magnets last is that the rotor is easy to install in to the stator, but the disadvantage is that there is a risk of rotor unbalance.

In this prototype building project it was decided to assemble the magnets first. Due to magnetic forces the rotor needs to be installed inside the stator using special tools to avoid the rotor hitting or jamming on the stator. Before assembling the magnets inside the rotor, it is necessary to check the position of magnet poles. The polarity of magnets can be marked on to the rotor endplate as in Figure 29.

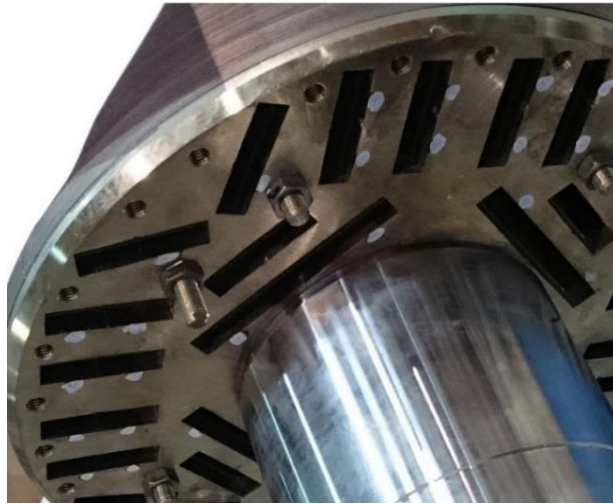


Figure 29. Rotor front endplate prepared with markings to show the magnets places and the magnets polarity in relation to the magnet slots.

From Figure 29 can be seen that every magnet slot does not have a marking which means that these slots are left empty without magnets.

Before beginning in the magnet assembly, it is important to wear on the personal safety equipment as specially eye protectors and protective gloves. The magnets have a porous structure and if a magnet brakes it will crack in to a several small pieces which have high risk to fly all over. In Figure 30 is an example of two broken magnets which were hit to each other as a result of magnetic pull.



Figure 30. Two damaged magnets which was hit to each other.

Magnet polarity check is needed to be done before magnets are assembled inside the rotor. In this prototype building it was noted that the magnet manufacturer had made a marking with a black pen one side of the magnets, as can be seen in Figure 31.



Figure 31. Magnet with a polarity marking on one side of it.

Even though the magnets had markings, the magnet polarity for each different packing was tested against a test magnet to ensure that all magnets polarities markings correspond to each other.

Tools that are needed in the magnet assembly are pliers which have a good grip on the magnet and a pushing tool to get the magnets inside to the rotor. The assembly tools should be manufactured from stainless steel to avoid the magnets sticking on the tools. To ensure a robust design of rotor, the magnets are bonded firmly into the magnet slots with a suitable heat resistant glue.

The magnet assembly begins by pressing glue inside the rotor slot as presented in Figure 32a and inserting the magnet into the magnet slot with pliers as presented in Figure 32b.

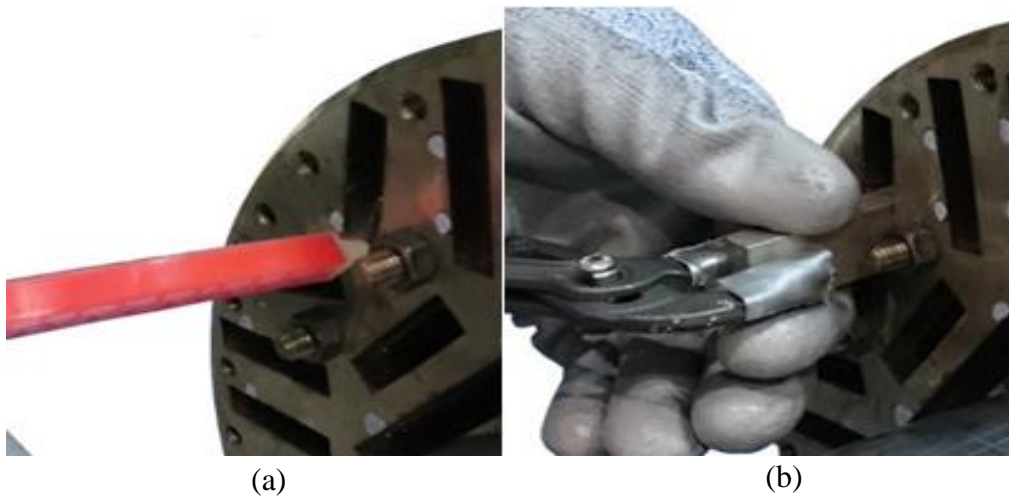


Figure 32. Magnet assembly where glue is pressed in to the magnet slot (a) and magnet is inserted in to the magnet slot (b).

After glue and the magnet are inserted into the slot the magnet is pushed against to the rotor back endplate with magnet pushing rod as in Figure 33a. The assembled magnets can be inspected from the rotor back endplate's holes to ensure that the magnets are perfectly at the end of the slot, as presented in Figure 33b.

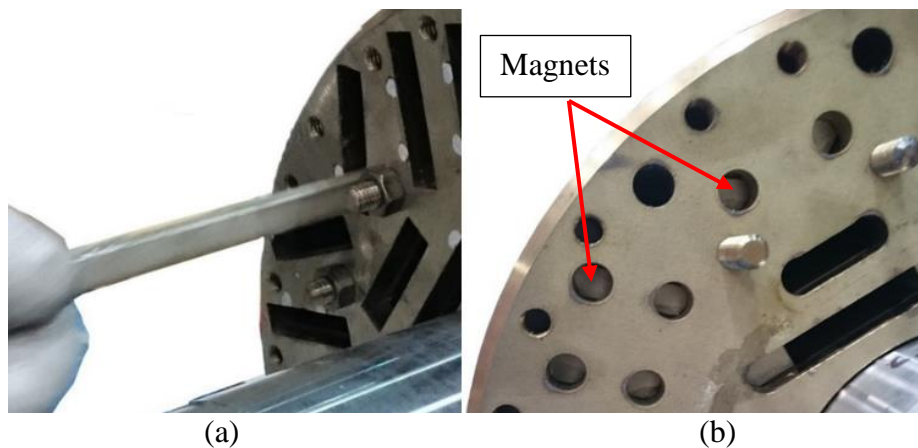


Figure 33 Magnets assembly procedure where magnets are pushed to the bottom of the magnet slot (a) and magnets are inspected from the back endplate to be in the bottom of the slot (b).

When number of magnets increases in the rotor it needs to be noted that the magnetic forces of the rotor increases. The magnetic forces affect that soft magnetic materials for

example tools made of black steel is in attraction to the rotor. There is also a potential risk to work near the magnetic rotor if person has a pacemaker (Haapala 2011: 26).

When all the magnets are assembled inside the rotor as presented in Figure 34a the rotor front endplate can be sealed with the magnet assembly glue as presented in Figure 34b to give a more robust design and to protect the magnets.

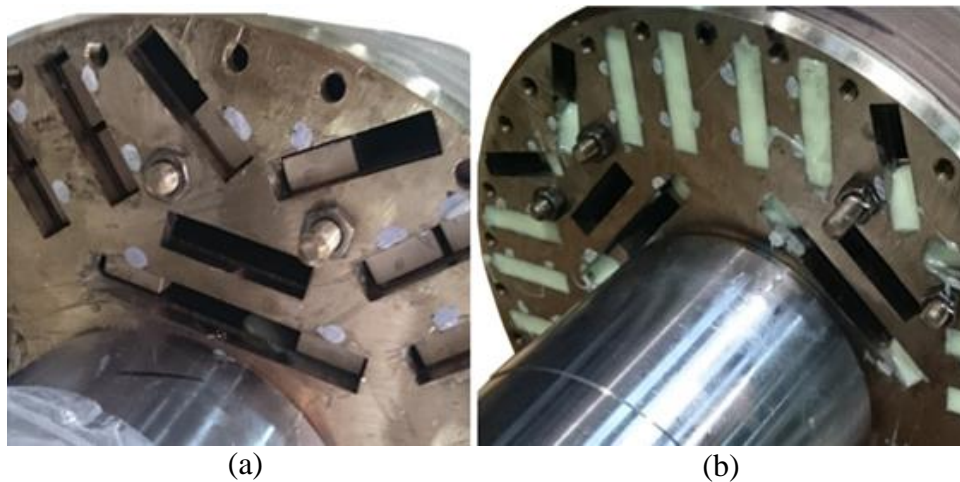


Figure 34. Rotor front end when all the magnets are assembled in to the rotor (a) and sealed with two component epoxy (b).

When the magnet assembly glue is dry enough based to the material's technical instruction, the rotor can be balanced. Before balancing the rotor, cooling wings which are manufactured from stainless steel are fixed to the stud bolts in rotor endplates, as presented in Figure 35.

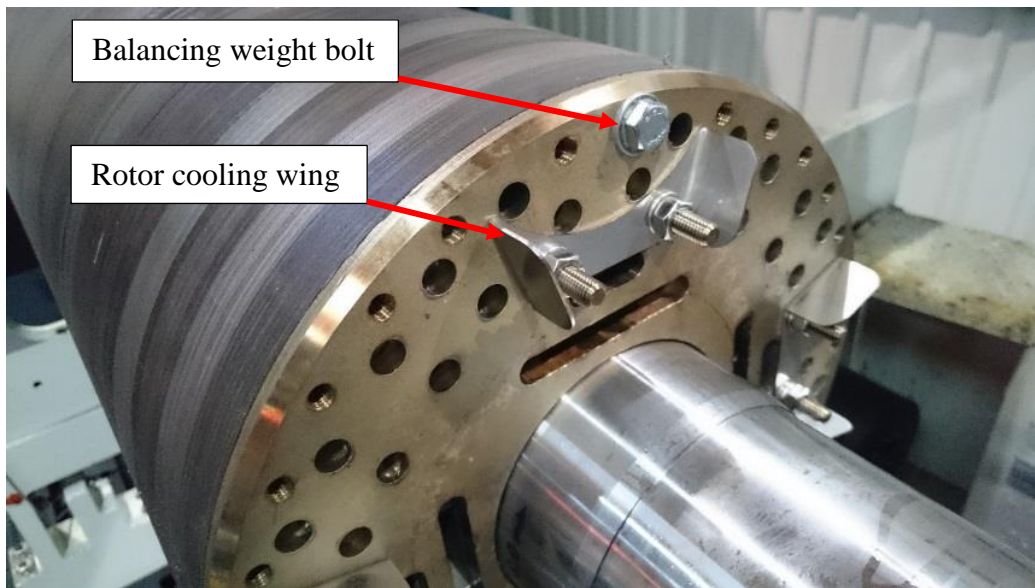


Figure 35. Rotor in a balancing bench where can be seen the rotor cooling wings and the one balancing weight.

When the rotor is moved to the balancing bench, careful handling of the rotor is needed because of the magnetic forces. Rotor balancing is done to reduce vibrations that could affect for example a bearing damage when the motor is running. ISO 21940-12:2016 standard defines the different rotor balancing grades for electric motors which eases the prototype building by just following the standard. In this prototype development process, we selected balancing precision grade G 2.5. The rotor is balanced in a balancing bench by adding weight bolts to the rotor endplate as can be seen in Figure 35.

6.5 Rotor magnetic forces effect on assembly process

Permanent magnet rotor assembly inside the stator may cause safety issues or material damages because of the rotor magnetic forces. For safe working and avoiding any material damages it is recommendable to use special rotor assembly tools to control the rotor movements. In rotor assembly process in to the stator, there affects two different kind of magnetic forces of which one is in axial direction and another in the radial direction, as presented in Figure 36.

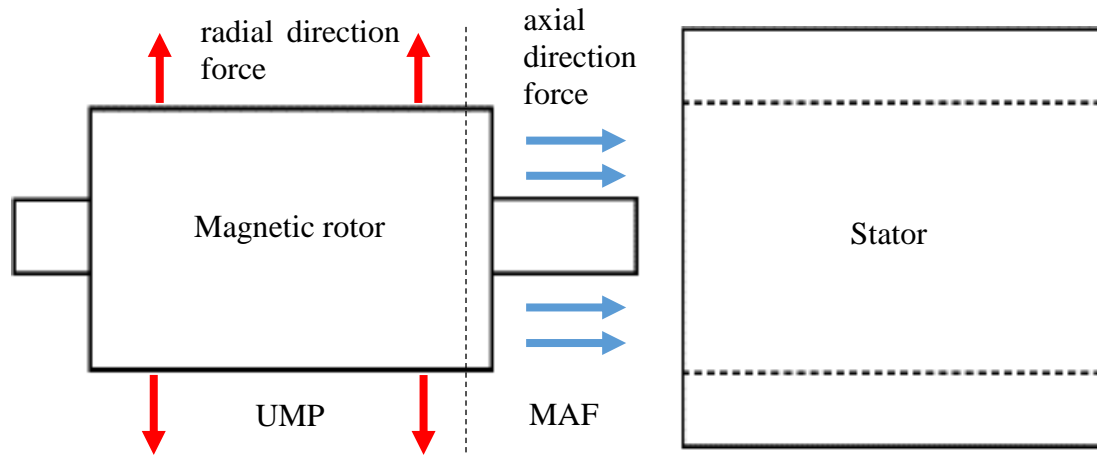


Figure 36. Magnetic forces in the rotor assembly procedure in to the stator.

The axial direction force is also called as magnetic assembly force (MAF) which tries to pull the rotor inside the stator in axial direction and is vanished when the rotor and stator are axially aligned. The radial direction force is called as unbalanced magnetic pull (UMP) and it tries to pull the rotor against to the stator core in the radial direction. (Lee, Hong, Woo, Park, Choi, Nam 2012: 1).

This thesis also examines if it is possible to reduce the rotor magnetic forces in the assembly process by short circuiting the rotor fluxes. To inspect if the rotor magnetic forces is possible to reduce, the rotor is modeled without and with iron rods inside the empty magnet slots by two-dimension FEM modeling, to calculate open circuit voltage and air gap flux density. The two-dimension FEM is modeled on the rotor radial direction which gives the results for UMP. In the rotor assembly process the rotor in actual fact does not have any radial direction velocity, but to calculate the rotor's produced open circuit voltage and air gap flux density in two different cases, FEM modeling is done by using 1800 rpm rotor running speed inside the stator. The first model in Figure 37 is rotor with empty magnet slots at speed of 1800 rpm.

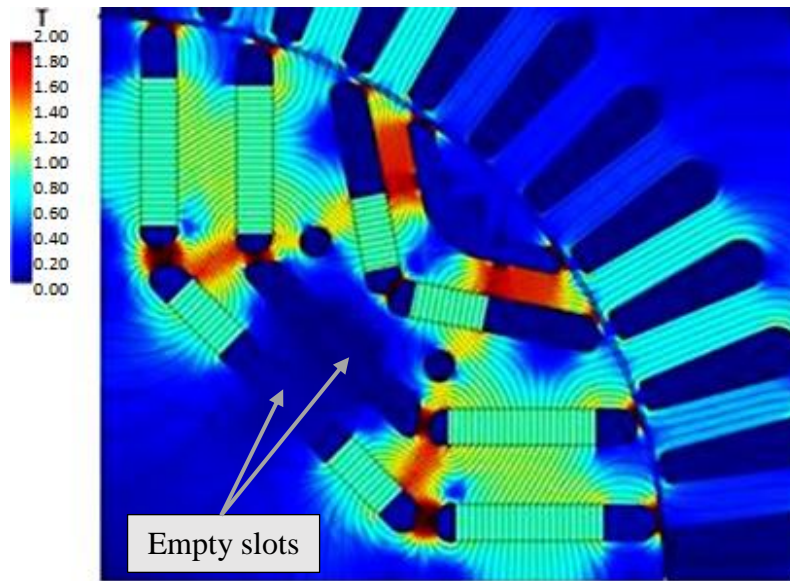


Figure 37. Modelled fluxes with speed of 1800 rpm when rotor has empty magnet slots.

In Figure 37 the empty magnet slots do not have flux lines and the flux density

$$B = \mu_r \mu_0 H, \quad (11)$$

is about zero when μ_r is the relative permeability of magnetic material which is air, μ_0 is the permeability of free space and H is the strength of magnet field. Relative permeability of air is 1.00 and permeability of free space is $4\pi \cdot 10^{-7}$ H/m. The magnetic field is produced by the permanent magnets inside the rotor.

Figure 38 presents the model where empty magnet slots are filled with iron rods which creates magnetic paths. Magnetic paths are created because of high relative permeability of iron material as can be seen from Appendix 3. From Figure 38 it can be noted that the flux lines pass through the iron filled slots and this area has increased flux density when compared to the model in Figure 37. The increased flux density in the iron filled slots area has decreased the flux density in the air gap between rotor and stator core and in the stator core teeth.

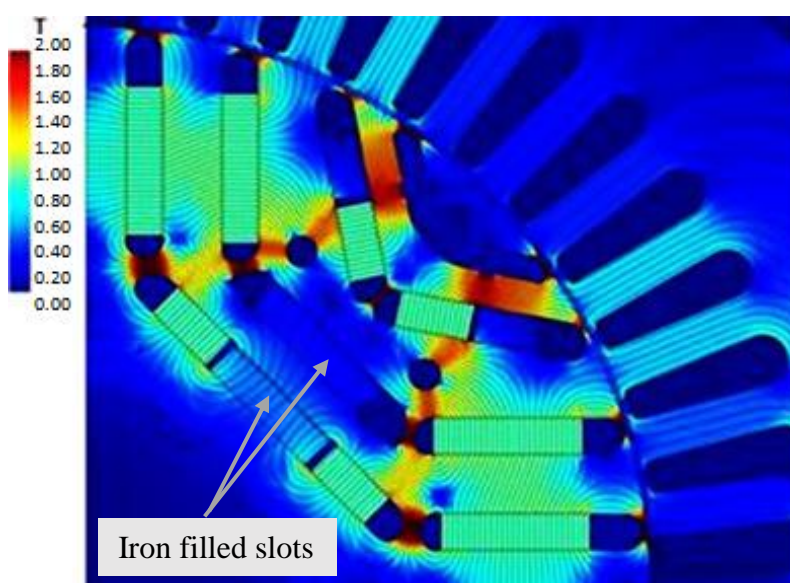


Figure 38. Modelled fluxes with speed of 1800 rpm when the empty magnet slots are filled with iron rods.

The two-dimension FEM simulations results of rotor with empty slots and iron filled slots at running speed of 1800 rpm is presented in Table 4.

Table 4. Simulated open circuit voltage U_{oc} and flux density in the air gap B with empty magnet slots and iron filled magnet slots at speed of 1800 rpm.

Model	U_{oc} (V)	B (T)
Empty slots	169.3	0.422
Iron filled slots	139.4	0.350

From Table 4 it can be noted that the simulation model where slots are filled with iron have decreased open circuit voltage and air gap flux density, if compared to the model with empty slots. As the motor open circuit voltage depends on the external magnetic field of the rotor (Pyrhönen etc. 2014: 45–46), it means that the empty slots filling with iron rods decrease the external magnetic field.

The effect of using iron rods inside the rotor core for decreasing the rotor magnetic forces in the assembly process, can be also inspected with the flux densities presented in Table 4 by applying the Maxwell's stress tensors magnetic part

$$\sigma_n = \frac{1}{2} \mu_0 (H_n^2) = \frac{1}{2} \mu_0 \left(\frac{B_n}{\mu_0} \right)^2, \quad (12)$$

where μ_0 is permeability of vacuum and B_n is the normal direction magnetic flux density in air gap as presented in Figure 39.

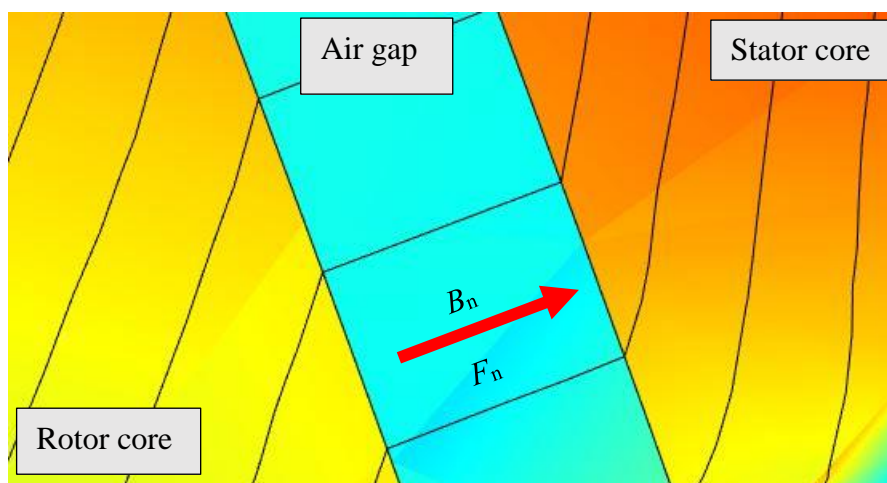


Figure 39. Air gap flux density in normal direction B_n , normal direction force F_n and flux lines.

The air gap flux density has a tangential and a normal direction component but for simplicity the tangential component is assumed to be zero. The mutual normal direction force F_n in the air gap between rotor and stator core in Figure 39 can be solved as

$$F_n = S \sigma_n \left(1 - \frac{1}{\mu_{r,M350-50A}} \right), \quad (13)$$

where S is the air gap area between rotor and stator surfaces and $\mu_{r,M350-50A}$ is the relative permeability of rotor and stator core material (Pyrhönen 2014: 32–35). Rotor and stator

core are manufactured from M350-50A electric steel which has relative permeability of 1020 at 1.5 T (Cogent Power 2002: 6). The mutual normal direction forces between magnetic rotor and the stator are calculated by assuming a situation where 25 % of the rotor's full length is assembled inside the stator. The calculated normal direction force F_n between rotor and stator core are:

- With empty slots 10.7 kN
- With iron filled slots 7.4 kN.

When inspecting the calculated normal direction forces, defined also as UMP, it needs to remember that flux densities used in the calculations are modelled with rotating magnetic field, which results that the calculated forces are not authentic in the assembly procedure. The calculated forces indicate that filling the empty magnet slots with iron are due to 31 % decreased radial direction force between rotor and stator.

Based to the FEM analysis results of decreasing rotor magnetic forces, it is decided to examine in practice if the rotor assembly forces are decreasing by filling the empty slots with iron rods as presented in Figure 40.

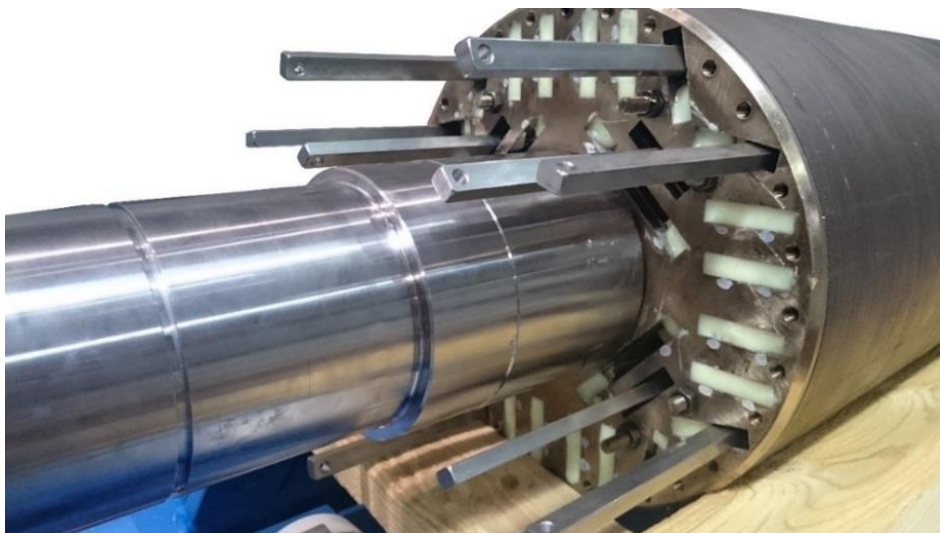


Figure 40. Iron rods assembled inside to some of the empty magnet slots.

6.6 Magnetic rotor assembly inside the stator with special assembly tools

Rotor that has magnetic forces may require special assembly tools to control the rotor movements in assembly process. The assembly tools are generally called as jigs and the purpose is to move controlled the rotor in axial and radial direction. In this prototype development project, we used one of the ABB Motors and Generators in Vaasa permanent magnet rotor assembly jig. The assembly jig consists of a rotor height adjustment tool which controls the radial direction magnetic pull force. The rotor height adjustment jig is presented in Figure 41 when the rotor is being set down on it.

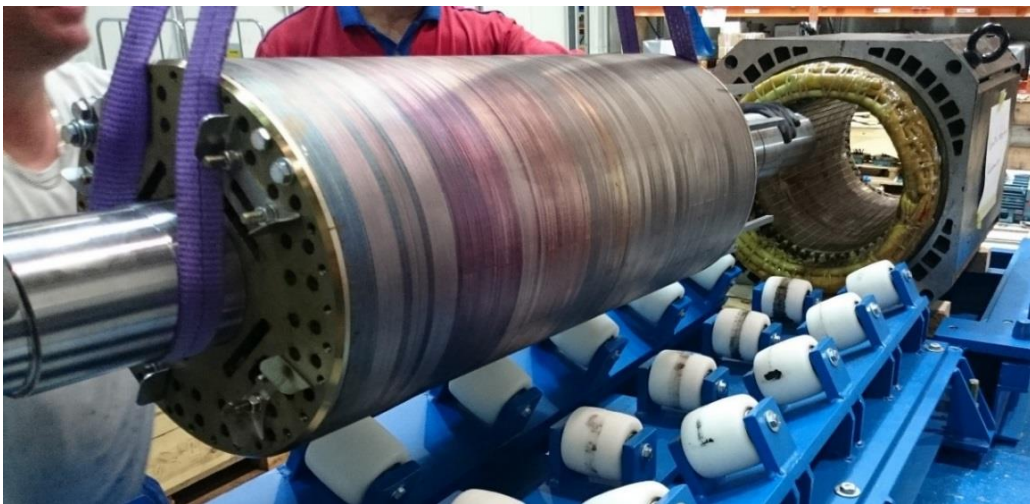


Figure 41. Rotor height adjustment jig with nylon rollers when PMASynRM prototype rotor is set on it.

The rotor height adjustment jig has bearing mounted nylon rollers to protect the rotor core surface in the mounting procedure and to enable rotor smooth control on the axial direction. The height adjustment jig has adjustable feet to set the rotor vertically to correct level in relation to the stator.

Axial direction magnetic forces are controlled with axial adjustment jig. The axial adjustment jig consists of a body, which is fixed to the stator body and of a long adjustment threaded rod which travels, through the center of the jig body, as presented in Figure 42. The end of the long adjustment threaded rod is fixed in to the rotor shaft threads. The threaded rod's job is to pull the rotor controlled in to the stator.

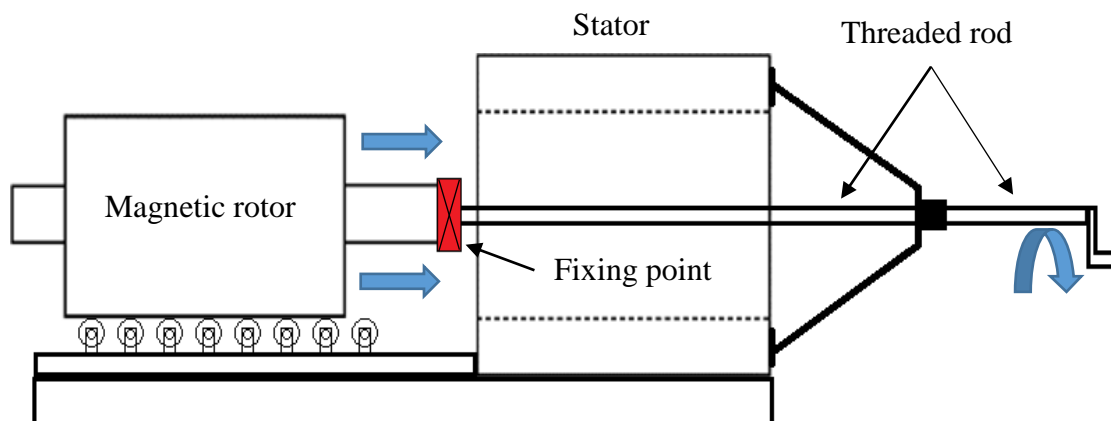


Figure 42. Assembly jig with a threaded rod pull instrument assembled to the rotor shaft through the stator.

The magnetic rotor is pulled inside the stator in the blue straight arrows direction shown in Figure 42, when rotating the threaded rod in the blue curved arrow direction.

After the rotor is installed inside the stator as in Figure 43, the next step is to check if some sensors, for example temperature sensors are needed to be installed to the winding.

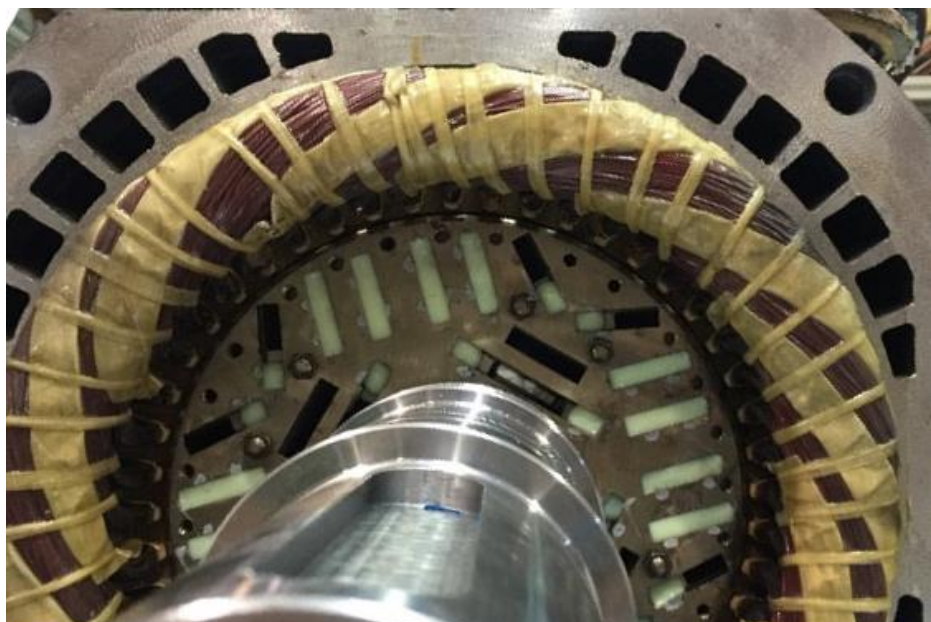


Figure 43. PMSynRM prototype rotor assembled inside the HDP series 250 frame size stator.

At last the bearings, endshields, terminal box and the external cooling fan motor are assembled. In this PMSynRM prototype we used standard bearings because the test run time is only some hours. Normally, with motor in VSD use insulated bearing at N-end should be used, because of bearing currents from converters harmonics (Hyvönen 2016: 16).

7 METHODS AND RESULTS USED IN PROTOTYPE MEASUREMENT

Measurements for the HDP 250 PMaSynRM prototype are done at ABB Motors and Generators, Vaasa test area. The PMaSynRM prototype tests are done using ABB's manufactured direct torque control frequency converter ACS880-17-1950A-7, frame 3xD8T+4xR8i with nominal voltage 525–690 V and nominal current 1950 A. PMaSynRM measurement results are compared to the HDP 250 induction motor with aluminum squirrel cage. The induction motor has also been tested at ABB Motors and Generators in Vaasa. The induction motor is tested in DOL at 500 kW and 575 kW. The PMaSynRM prototype is designed for constant torque and constant power use. At low running speed range, the motor is driven with constant torque and at the high running speed range with constant power. Figure 44 shows the PMaSynRM assembled in the test bench.

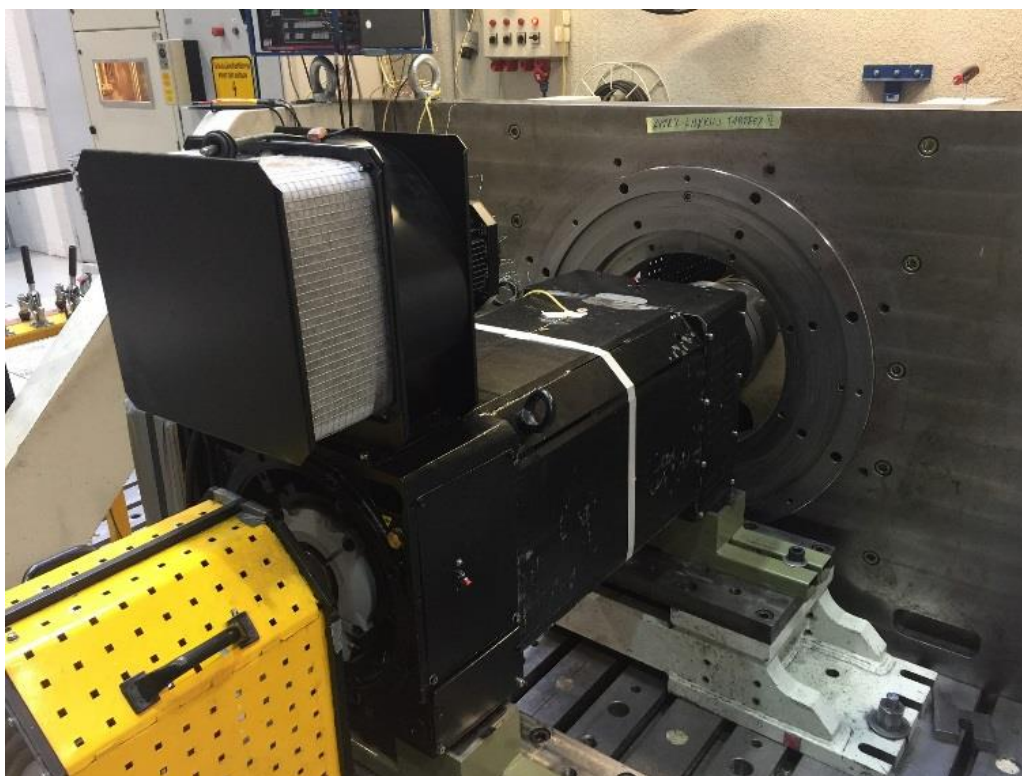


Figure 44. HDP 250 PMaSynRM fixed to the test bench, D-end shaft fixed to the load machine and N-end shaft is protected with a cover.

7.1 Measurement methods and results of PMaSynRM and IM

The measurements begin from fixing the motor on to the test bench and fixed to the load motor which acts as a generator. Load motor used in the measurements is ABB's manufactured AMI 560M4P BSFTXYH squirrel cage motor which generates the electrical energy back to the network. Temperature sensors are attached to the measurement surfaces of PMaSynRM. ACS880 converter power cables are connected to the motor terminal box in delta connection.

PMaSynRM N-end shaft is protected with a cover which was presented in Figure 44 as the yellow coloured cover. In the measurements it needs to be noted that even when the PMaSynRM is not powered but it is still running, it generates voltage on to the connection terminals because of the magnets in rotor.

In the beginning of the prototype test, PMaSynRM induced open circuit voltage is measured at ambient temperature by rotating the PMaSynRM with load motor. The results of PMaSynRM measured and simulated open circuit voltages are presented in Section 8.1.

The measured test results for PMaSynRM fed with ACS880 and IM in DOL use are presented in Table 5 in the form of load type as constant torque and constant power. In the Table 5 U_{acs} is the sinusoidal supply voltage for FC and U_{mot} is the first harmonic of motor supply voltage. In Table 5 η_{mot} is motor efficiency, η_{acs} is FC efficiency and η_{tot} is the total efficiency of motor and FC. The last four columns in Table 5 are temperature rises in Kelvins where $\theta_{Cu,max}$ represents stator end winding, θ_{fr} motor frame, θ_{db} D-end bearing and θ_{rt} rotor surface. Temperature rises are measured only for some operating points because each temperature rise test takes time for several hours. Temperature rise tests are done based to the IEC 60034-1 standard, for specified output power levels and running speeds. In the temperature rise test the motor is running as long as the measured temperature have stabilized, which means that the temperature rise is less than 2 °C/h.

Table 5. Measurement results of PMSynRM with ACS880 and IM in DOL use.

P_{out} (kW)	n (rpm)	T (Nm)	U_{acs} (V)	U_{mot} (V)	I (A)	$\cos\phi$	η_{mot} (%)	η_{acs} (%)	η_{tot} (%)	$\theta_{Cu, max}$ (K)	θ_{fr} (K)	θ_{db} (K)	θ_{rt} (K)
PMSynRM fed with ACS880													
150.7	525	2730	531	124	820	0.90	93.2	88.9	82.8	52	37	18	68
301.0	1050	2730	526	250	824	0.87	94.9	93.8	89.0	73	57	30	131
302.3	1800	1593	527	382	521	0.90	96.0	95.0	91.2	55	50	22	105
301.3	2400	1194	-	472	413	0.92	96.1	95.6	91.9	-	-	-	-
302.3	3000	956	528	540	353	0.96	95.1	96.3	91.6	-	-	-	-
250.5	525	4548	528	138	1315	0.85	91.8	90.9	83.4	-	-	-	-
501.2	1050	4548	527	276	1318	0.83	94.5	94.5	89.3	-	-	-	-
501.7	1800	2653	524	429	807	0.86	96.3	96.4	92.8	87	76	31	130
501.3	2400	1990	-	534	627	0.89	97.2	97.1	94.4	-	-	-	-
502.6	3000	1593	-	531	575	0.92	96.4	97.1	93.6	-	-	-	-
200.6	525	3638	528	132	1062	0.87	92.7	90.4	83.8	-	-	-	-
400.8	1050	3638	528	266	1068	0.84	94.9	94.4	89.6	-	-	-	-
402.6	1800	2122	524	409	664	0.88	96.4	95.8	92.4	-	-	-	-
400.4	2400	1592	-	507	520	0.90	96.9	96.5	93.5	-	-	-	-
403.0	3000	1273	528	534	462	0.98	96.0	96.9	93.0	-	-	-	-
300.6	525	5460	525	140	1599	0.84	90.1	90.8	81.8	-	-	-	-
601.7	1050	5460	524	286	1593	-	93.2	94.4	88.0	-	-	-	-
598.9	1800	3185	523	444	950	0.84	96.0	96.5	92.6	113	96	36.7	158
601.8	2400	2388	525	530	740	0.91	97.4	97.1	94.6	80	73	23	100
601.2	3000	1910	527	524	696	0.98	96.6	97.2	96.6	95	94	29	144
Induction motor in DOL use													
501.1	1781	2687	-	401	873	0.87	95.1	-	-	93	92	42	179
573.0	1773	3066	-	400	991	0.89	94.2	-	-	140	126	42	239

7.2 PMSynRM voltage, current and torque

Figure 45 shows the relationship of measured voltage, torque production and current as a function of running speed. The measured results are presented in a load type form as constant torque and constant power. Constant torque is used at 525–1050 rpm and constant power at 1050–3000 rpm. The relationship of output power, torque and running speed in constant torque and constant power presentation can be explained with Equation 1.

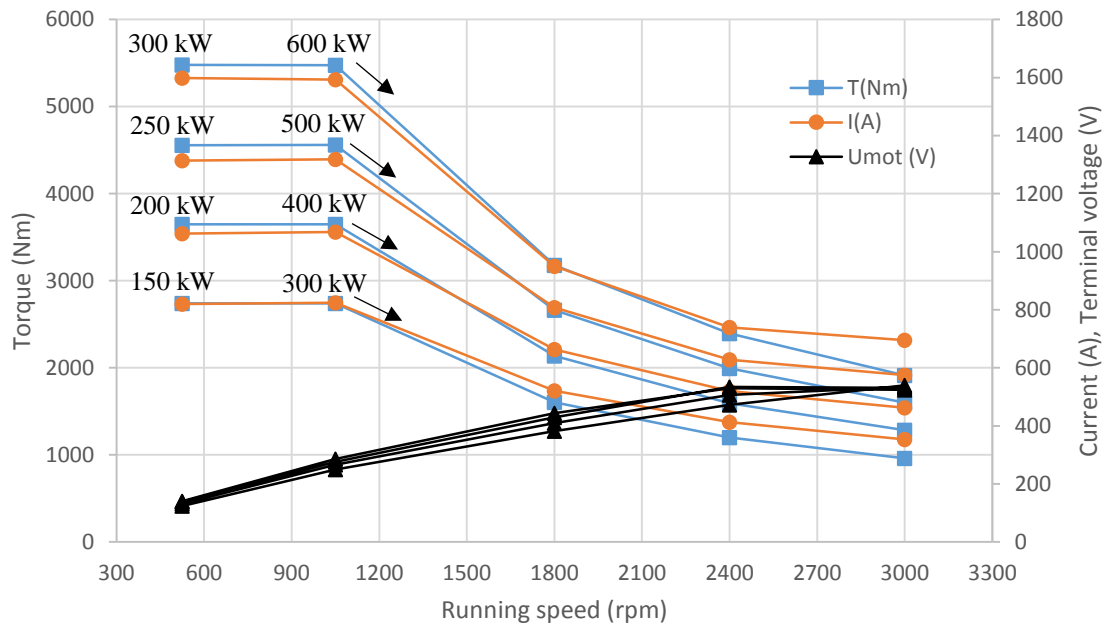


Figure 45. PMSynRM torque, current and voltage presented in the form of constant torque and constant power with the function of running speed.

At field weakening area from 2400 rpm to 3000 rpm the voltage stabilizes because the limitation of supply voltage. Also, the current stabilizes related to voltage because power is constant and voltage and current has relationship to power as

$$P = \sqrt{3}UI \cos \varphi, \quad (14)$$

where U is voltage and I is motor current.

From Figure 45 it can be seen that with high values of output power for example at 600 kW the voltage increases linearly with running speed up to 2400 rpm which is the field weakening point. It can be also noted that with low output power for example at 300 kW the voltage increases linearly with running speed up to 3000 rpm. It means that with 300 kW output power the field weakening point is at higher running speed than 2400 rpm as it is with 600 kW.

7.3 Efficiencies and temperature rises of PMaSynRM and IM

The measured total efficiency of PMaSynRM & ACS880 and the partial efficiencies of PMaSynRM and ACS880 are presented at 60 Hz frequency in Figure 46. The PMaSynRM efficiencies are also compared to the earlier measured results of IM efficiencies at 60 Hz sinusoidal frequency in DOL use.

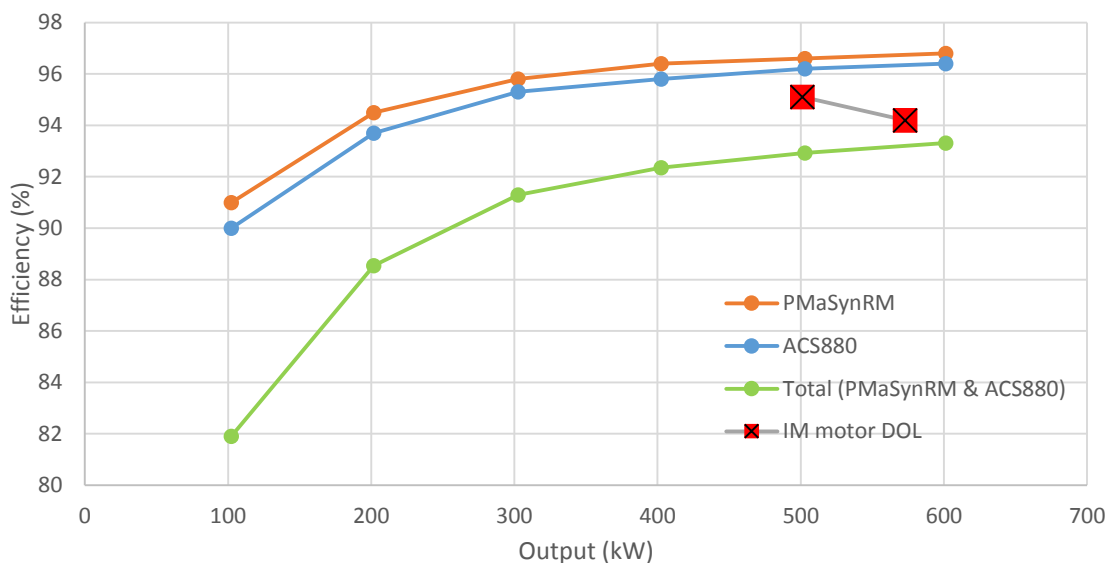


Figure 46. Measured efficiencies of PMaSynRM, ACS880, total efficiency of PMaSynRM with ACS800 and efficiency of IM with 60 Hz supply frequency.

From Figure 46 it can be seen that the efficiency of PMaSynRM increases with the function of output power as the induction motor efficiency decreases strongly with the function of output power. It can be also noted that ACS880 efficiency behaves the same way

as PMSynRM efficiency with a function of output power, even though the efficiency of ACS880 is a bit lower. When output power is increased the ACS880 efficiency approaches the manufacturers given nominal power efficiency of 97 %, which can be found from Appendix 4. The total efficiency of PMSynRM & ACS880 is lower than the IM efficiency in DOL use.

The PMSynRM increasing efficiency with the function of output power can be partly explained with the spatial harmonics of voltage and current. Figure 47 presents the converter-fed terminal voltage and current waveforms from PMSynRM connection terminal at 100 kW test run with 100 Hz frequency which is outside the field weakening area. The voltage and current at 100 kW output have lots of harmonics which cause iron losses and additional losses, as was discussed in Section 2.6. No extra filters were used with ACS880.

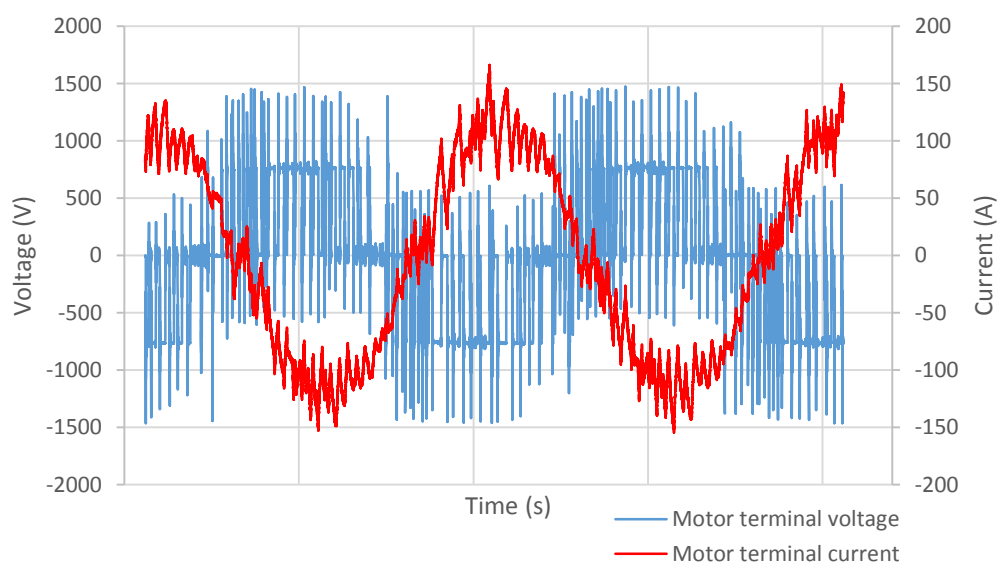


Figure 47. Measured converter-fed PMSynRM terminal voltage and current before field weakening area at 100 kW with 100 Hz frequency which corresponds to 3000 rpm running speed.

Outside field weakening area for example at output power 600 kW and running speed less than 2400 rpm, the voltage and current waveforms are mostly like in Figure 47 which causes iron losses and additional losses.

Figure 48 presents the measured converter-fed terminal voltage and current waveforms from PMSynRM connection terminal at 600 kW output power when the supply frequency is 100 Hz which corresponds to running speed 3000 rpm.

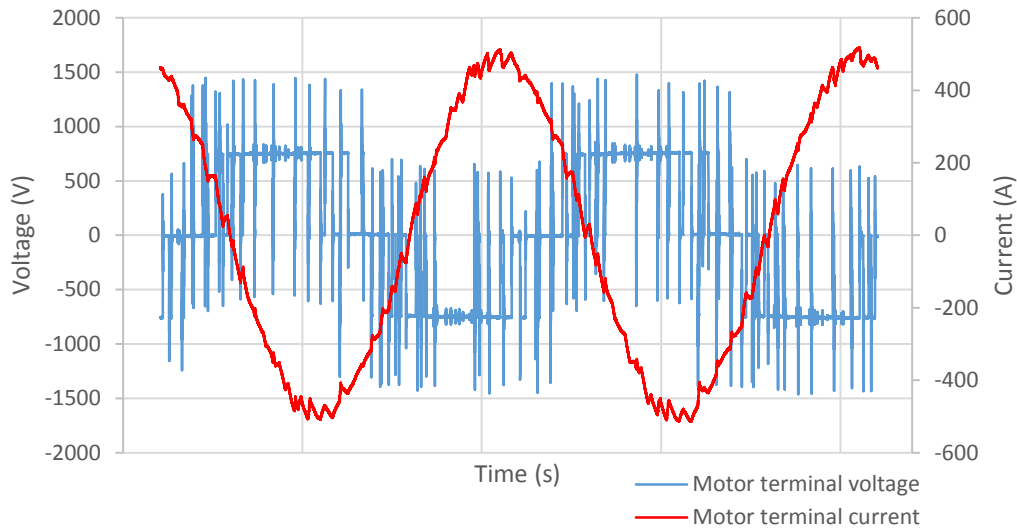


Figure 48. Measured converter-fed PMSynRM terminal voltage and current in field weakening area at 600 kW with 100 Hz frequency which corresponds to 3000 rpm running speed.

In Figure 48 the waveforms of voltage and current at field weakening area are much smoother than in Figure 47 which presents waveforms outside field weakening area. It can be stated that in field weakening area there are less iron losses and additional losses causing spatial harmonics.

Temperature rise of PMSynRM and IM is presented in Figure 49 with the function of output power at 60 Hz supply frequency which corresponds to running speed 1800 rpm. The temperature rise class B is 90 °C, F is 115 °C and H is 135 °C as defined in Section 2.7.

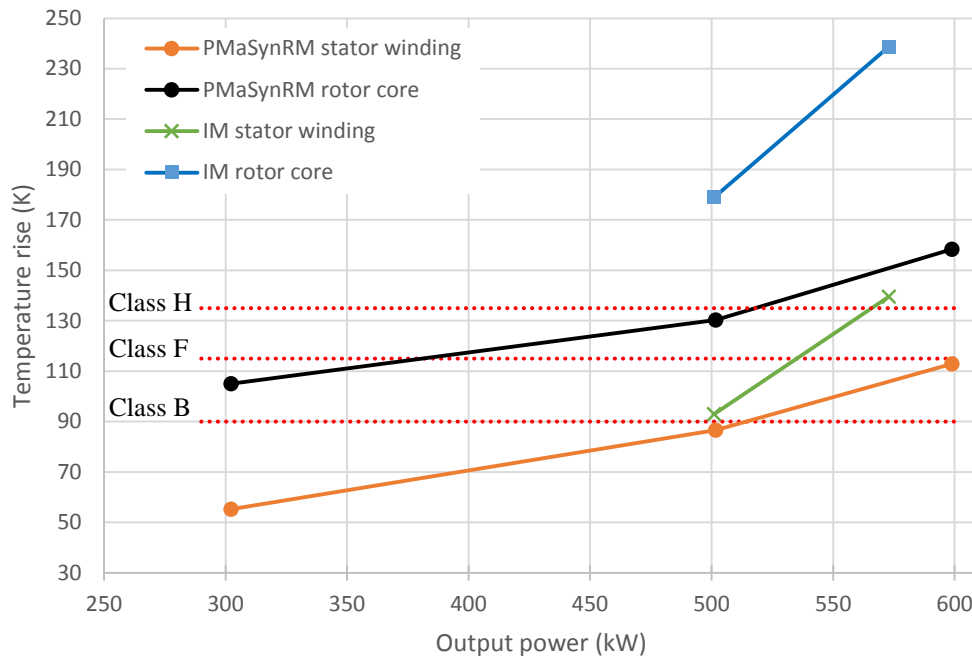


Figure 49. Temperature rise of stator winding and rotor core with the function of output power at running speed 1800 rpm. PMA SynRM is driven with ACS880 and induction motor in direct-online.

From Figure 49 it can be seen that PMA SynRM stator winding permissible temperature rise reaches the thermal class F on the full output power range. At 500 kW output the PMA SynRM stator winding permissible temperature rise reaches thermal class B. The IM stator winding permissible temperature rise does not reach the thermal class H at 575 kW output level. At 500 kW output level, the IM reaches thermal class F.

From Figure 49 it also can be seen that PMA SynRM rotor core surface temperature rise is on much lower level than in IM. For PMA SynRM the rotor temperature is critical because of the possibility of magnet material demagnetization. The maximum measured temperature of PMA SynRM rotor core surface is 158 °C and it does not reach the maximum allowable temperature of magnet $\text{Sm}_2\text{Co}_{17}$ Vacomax 225HR which is 350 °C.

PMA SynRM temperature rise of stator winding and rotor core at 600 kW output power with the function of running speed is presented in Figure 50.

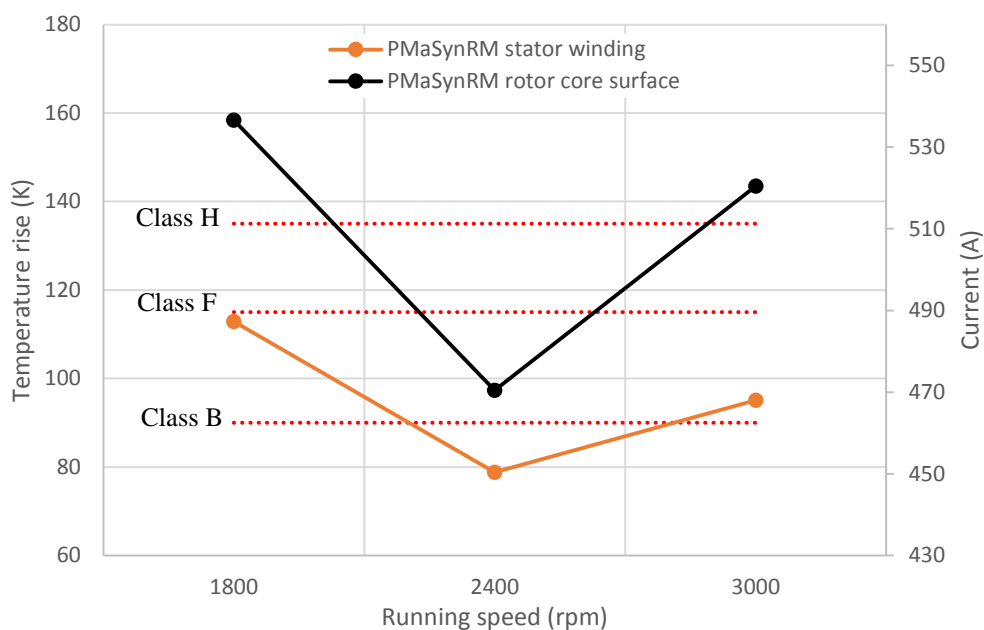


Figure 50. Temperature rise of PMSynRM stator winding and rotor core at 600 kW output power with the function of running speed.

From Figure 50 it can be seen that temperature rise of rotor core and stator winding at 600 kW output power decreases when moving from running speed 1800 rpm to field weakening area which is 2400–3000 rpm. Temperature rise at field weakening area is decreased because the level of frequency converters produced supply harmonics is low at field weakening area as was presented with Figure 48. When inspecting the temperature rise in the field weakening area from field weakening point 2400 rpm up to 3000 rpm, the rotor core and stator winding temperature rises. The rotor core temperature rises more than the stator winding temperature which is mostly affected from the iron losses because the supply frequency is increased for the running speed. Iron losses as hysteresis losses are in proportion to the frequency and eddy current losses are in proportion to the square of the frequency.

The PMSynRM temperature rise tests were also done by removing the air vent outlet cover from motor D-end which is presented in Figure 13. Air vent outlet cover cannot be removed in a normal use because of its IP protection properties. Reason to remove the air vent outlet cover was to inspect if the air flows better through the motor and if the temperature rise can still be decreased. The test was done at 600 kW output power with

running speed 1800 rpm. The temperature rise of HDP 250 PMSynRM is presented in Figure 51 with standard design and with removed air vent outlet covers.

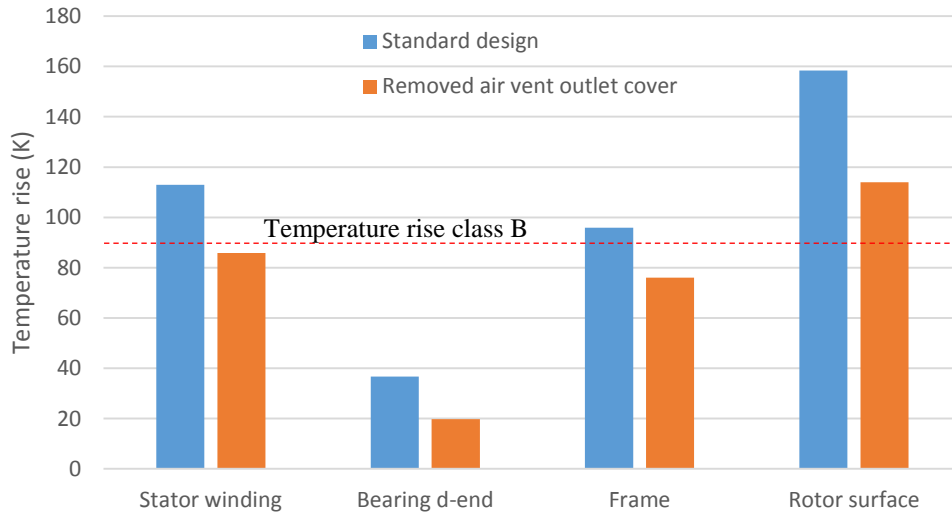


Figure 51. PMSynRM temperature rise with standard design and with removed air vent outlet covers at 600 kW output power with running speed 1800 rpm.

From Figure 51 can be noted that removing the air vent outlet covers the temperature rise of PMSynRM decreases noticeably compared to the standard design. Without air vent outlet covers the temperature rise class B is achieved at 600 kW output power with running speed 1800 rpm as the standard design reaches in temperature class F.

8 COMPARISON OF MEASUREMENT AND SIMULATION RESULTS

HDP 250 PMSynRM measured and simulated results are compared to inspect the accuracy of Adept FCSmek simulation software. Comparison is done with open circuit voltage, efficiency, current and power factor.

8.1 Open circuit voltage of HDP 250 PMSynRM

Open circuit voltage U_{oc} in HDP 250 PMSynRM is produced by the permanent magnets in the rotor. Open circuit voltages are measured by rotating the HDP 250 PMSynRM with the load motor at the beginning of the test run when the HDP 250 PMSynRM is at ambient temperature. The simulated and measured results of open circuit voltages are presented in Table 6 where can be noted that the simulated open circuit voltages are on a bit lower level than the measured open circuit voltages. Simulated open circuit voltages are averagely 7.6 % lower than the measured, which can be due to the different temperature, simulations inaccuracy or from other sources of error.

Table 6. HDP 250 PMSynRM simulated and measured open circuit voltages with different running speeds.

n (rpm)	Simulated U_{oc} (V)	Measured U_{oc} (V)
525	49.4	54.5
1050	98.8	106.0
1800	169.3	184.0
2400	225.8	243.0
3000	282.2	303.0
3600	338.7	-

8.2 Losses and efficiencies of HDP 250 PMSynRM

Efficiency is proportional to the total losses as can be noted from Equations 6 and 7. The simulated and measured efficiencies are presented with efficiency map as a function of supply frequency and torque. Efficiency maps are created with Gnuplot software by plotting data. The plotted measurement and simulation points are interpolated with Gnuplot software from a number of 30 points.

Efficiency map in Figure 52 presents the Adept FCSmek simulated efficiencies of PMSynRM in a DTC use. From Figure 52 can be noted that the highest efficiency area is divided in a large area in the middle of the efficiency map.

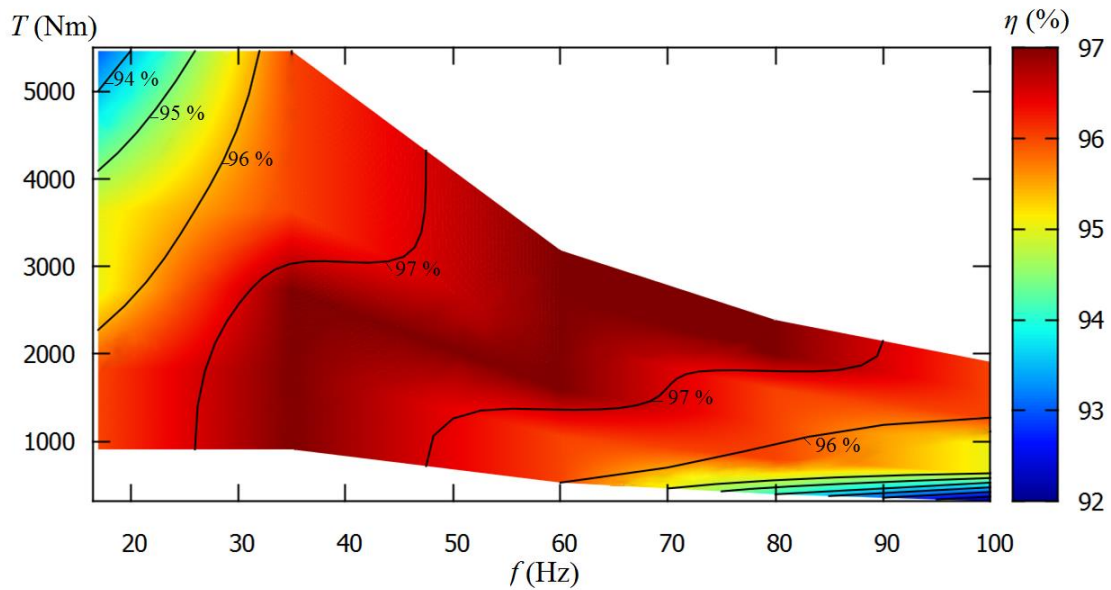


Figure 52. Simulated efficiency of HDP 250 PMSynRM in DTC use

Figure 53 presents the measured efficiencies of the PMSynRM fed with ACS880. From Figure 53 it can be noted that the measured highest efficiency area is more focused on 80 Hz supply frequency when torque is averagely 2400 Nm, which presents the field weakening point with high output levels as presented in Figure 45.

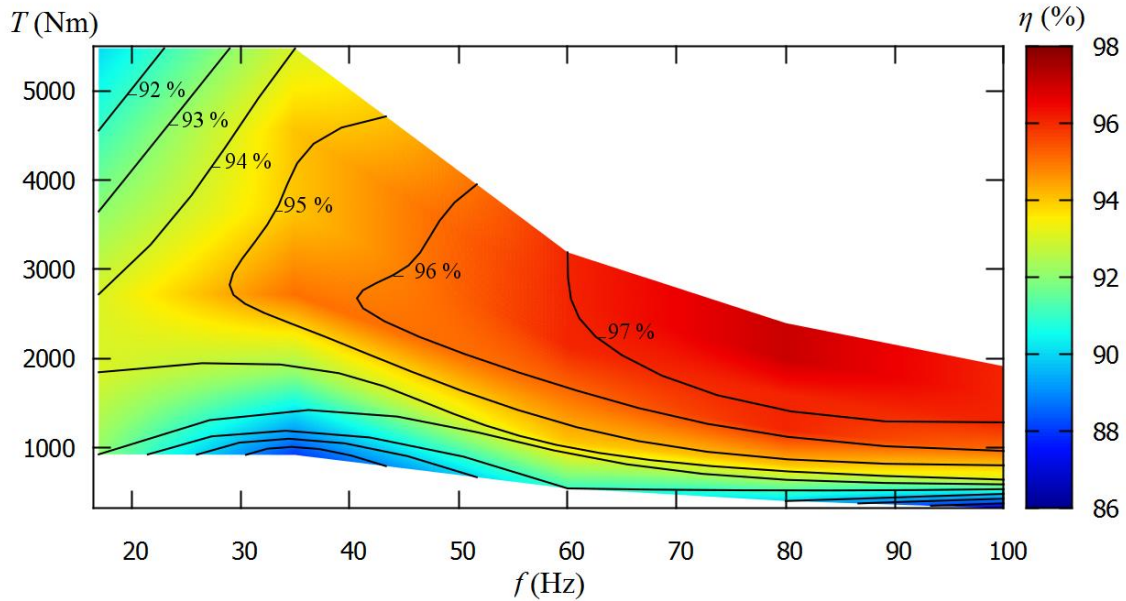


Figure 53. Measured efficiency of HDP 250 PMaSynRM in VSD use with ACS880 converter supply.

The difference on efficiency distribution as a function of supply frequency and torque in Figure 52 of simulated results and in Figure 53 of measured results can be explained with voltage and current waveforms of Figure 47 and Figure 48. The simulated efficiency results presented in Figure 52 have high efficiency in wide area because the simulations are done by Adept FCSmek which calculates every operating point in DTC use with an ideal voltage and current waveforms as in the field weakening area presented in Figure 48. The efficiency map of measured results in Figure 53 has high efficiency values focused only at the field weakening area, as the non-field weakening area has lower efficiency because of spatial harmonics waveforms of voltage and current as presented in Figure 47.

Figure 54 presents the measured total efficiency of PMaSynRM & ACS880 converter.

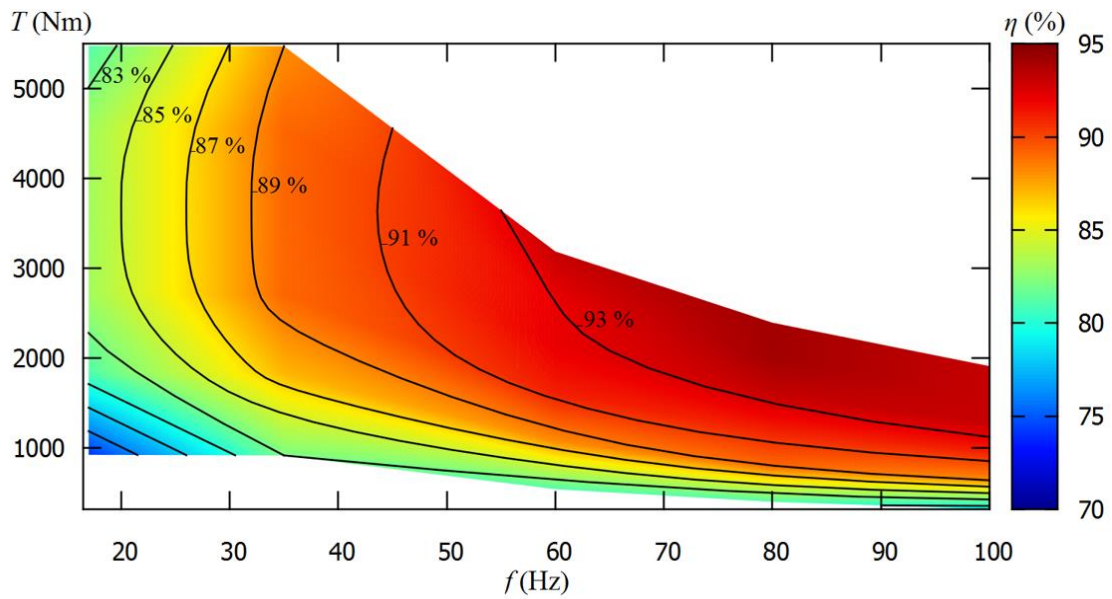


Figure 54. Measured total efficiency of HDP 250 PMaSynRM & ABB ACS880 converter.

From Figure 54 can be seen that the measured total efficiency of PMaSynRM & ACS880 is highest at the same area as the individually measured efficiency of PMaSynRM in Figure 53. The total efficiencies in Figure 54 are on a much lower level than the individually measured efficiency of PMaSynRM in Figure 53.

8.3 Power factor and current of HDP 250 PMaSynRM

Measured and simulated power factor and current of HDP 250 PMaSynRM are presented in Figure 55 with the function of running speed. It can be noted that the simulated power factor is at higher level than the measured power factor when inspecting running speeds 1050–2400 rpm, but at 3000 rpm the power factor is about on the same level.

The measured and simulated current in Figure 55 are about on the same level at running speed 1050 rpm. At the running speed 1800–3000 rpm the measured current is on a slightly lower level than the simulated current.

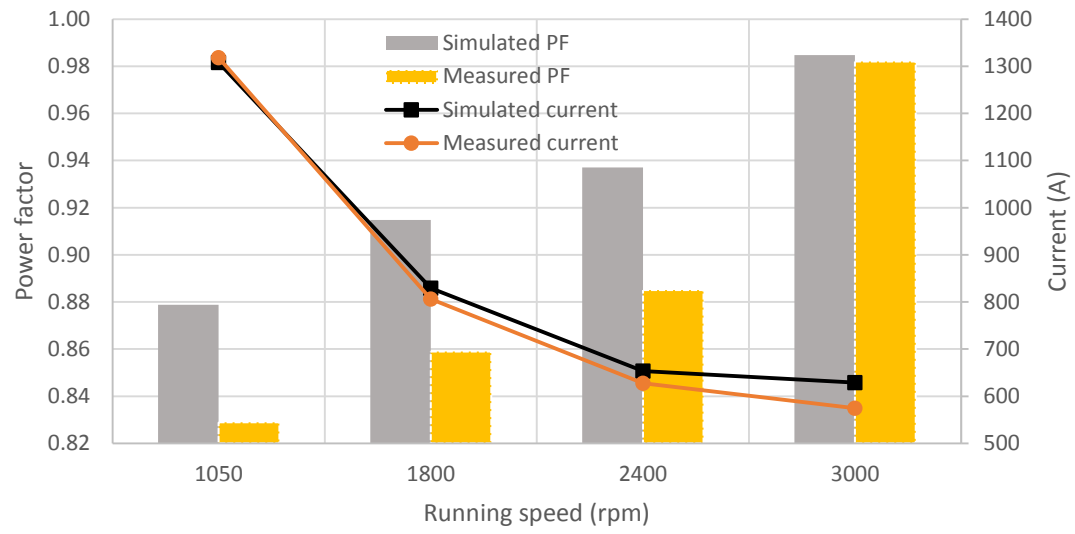


Figure 55. Simulated and measured power factor and current of HDP 250 PMaSynRM at 500 kW output power with the function of running speed.

9 SUMMARY AND DISCUSSION

Summary

The purpose of this thesis was to develop a HDP series 250 frame size PMSynRM and to find out if it has benefits on electrical and thermal properties compared to HDP series 250 size IM. The IM with aluminum squirrel cage have been designed and prototyped earlier with a target of 600 kW output power but it could only achieve 575 kW because of high temperature rise. The PMSynRM rotor is designed and assembled to an exactly same HDP 250 stator as the IM had.

Chapter 2 introduces the basics of non-excited synchronous motors from a view of PMSynRM. In Chapter 3 the ABB's HDP series motors are introduced and compared to an ABB's Process Performance series motor. PMSynRM prototype design methods are introduced in Chapter 4 to give a general view from the design process.

Based to the designed PMSynRM, calculations are done with Adept FCSmek to find out the voltage with lowest current for different operating points. Calculations are also done for the IM with aluminum squirrel cage, based to the earlier measured operating points. In Chapter 5 the PMSynRM simulation results and the IM simulation results are presented and compared to find out if the PMSynRM would have benefits on electrical and thermal properties. The simulation results of PMSynRM and IM in DOL and VSD use are presented in Table 3 at some output power levels. Both motors simulated losses in DOL use are presented in Figure 19, showed that PMSynRM has lower total losses than IM even if PMSynRM is inspected at 600 kW output power and IM at 500 kW output power. The higher loss production in IM compared to PMSynRM can be explained with rotor Joule losses which are only produced in IM. PMSynRM and IM loss production in sinusoidal DOL use are compared to VSD use in Figure 20, which shows that DTC supply increase losses in both motor types with all output power levels. Simulated efficiency of PMSynRM and IM in DOL and VSD use with different output power levels are presented in Figure 21 which shows that PMSynRM has higher efficiency in DOL and VSD use when compared to IM in DOL and VSD use. The simulated efficiencies in Figure 21

also shows that PMSynRM efficiency in DOL and VSD use stays constant when increasing output power as the IM efficiency in DOL and VSD use decrease strongly when increasing output power.

Based to the PMSynRM benefits found in the simulations according to electrical and thermal properties, the PMSynRM prototype was manufactured to verify the real measured properties. In Chapter 6 are described the PMSynRM prototype manufacturing process, which had many different kinds of steps on rotor manufacturing process and on rotor assembly process in to the stator.

After the prototype of HDP 250 PMSynRM was manufactured and assembled it was measured at the test area of ABB Motors and Generators in Vaasa, which is described in Chapter 7. The measurements were done with a load machine which acted as a generator and the PMSynRM was fed with standard ABB ACS880 DTC converter without filters. The PMSynRM measurements fed with ACS880 converter were compared to the earlier measured results of IM in DOL use. The measured total efficiency of PMSynRM & ACS880 was on lower level than the IM efficiency in DOL use as can be seen from Figure 46, where we can also see that the individual measurement of PMSynRM efficiency fed with ACS880 was on higher level than the IM efficiency in DOL use. The measured total efficiency of PMSynRM & ACS880 and the individual measured efficiency of PMSynRM and ACS880 increase with the function of output power as the IM efficiency decreases with function of output power, which also can be seen from Figure 46.

Temperature rise comparison of PMSynRM fed with ACS880 and IM in DOL use showed us that PMSynRM have better thermal properties than IM, as can be seen from Figure 49. PMSynRM prototype could operate at 600 kW output power as a result of temperature rise class F, as the IM could reach temperature rise class F only at 500 kW output power.

HDP 250 PMSynRM air vent outlet covers were removed from motor D-end, to examine if the flow of cooling air through the motor can be increased and if it has effect on thermal behavior. HDP 250 PMSynRM without air vent outlet covers achieved temperature rise

class B at 600 kW output power with 1800 rpm as the standard design with same ratings achieved temperature rise class F as can be seen from Figure 51.

In Chapter 8 the HDP 250 PMSynRM measurement results are compared to Adept FCSmek calculation results to review the accuracy of simulation software. The simulation results of open circuit voltages are averagely 7.6 % lower than the measurement results. In the efficiency maps of simulated efficiencies in Figure 52 and the measured efficiencies in Figure 53, have difference on the area of highest efficiency with the function of running speed and torque. The simulation results efficiencies in Figure 52 have a wide high efficiency area as the measurement results efficiencies in Figure 53 are focused on the field weakening area. The difference in the efficiencies of simulation results are caused from the Adept FCSmek simulation software, which does not take into account spatial harmonics outside the field weakening area, which cause iron and additional losses.

Current and power factor measurement and simulation results are compared at 500 kW output power with the function of running speed as can be seen from Figure 55. The measured and simulated current difference is minimal with small running speed but it increase when increasing running speed. The simulation and measurement results of power factor has some difference with running speeds 1050–2400 rpm but with maximum speed at 3000 rpm the difference is minimal.

Discussion

One of the questions raised up due the prototype manufacturing process was that if IP23 is enough to protect the HDP series motor against metal dust when there is a magnetic rotor inside. The HDP motor with IP23 has a fabric filter on its cooling intake and it should prevent any metal dust getting inside the motor. Also, a question was raised which kind of tools should be used in PMSynRM manufacturing as there are magnetic forces. It was decided that the assembly tools should be made of stainless steel to avoid them to get pulled against the motor surface and thus to ease the manufacturing process.

When inspecting the permanent magnet glue properties, it was noted that more heat resistant glue should be used, although it worked well on the test run. The glue is easy to change for a more heat resistant type.

The rotor magnetic assembly forces was simulated due to result of 30 % decrease in radial direction force between rotor and stator. In practice, using the iron rods inside the rotor in the assembly process was not found any effect on reducing the rotor magnetic assembly forces. The PMM assembly jig which was exploited in the PMSynRM prototype assembly process found not to be a perfect size but it became good enough with few modifications. If mass-produced large series of motors with magnetic rotors are designed, it would be profitable to design a new assembly jig of right size.

In the test field measurements we noted difficult to find out the correct frequency converter speed proportion gain values to start the motor and to change the running speed. The PMSynRM had some magnetic vibration noise because of the wrong speed proportion gain value. It was found to be working well when correct speed proportion gain value was found as in start were used small speed proportion gain values and for stable full load operation speed proportion gain values were increased. Tachometer added to the PMSynRM could be useful to run the motor smoothly by giving running speed information for the frequency converter.

The PMSynRM could be driven at 600 kW output power as the IM could be driven only at 575 kW because of high temperature rise. At 600 kW output power the maximum rotor temperature rise was 158 K, which means for example with 25 °C ambient temperature 183 °C for rotor temperature. The permanent magnets used in this PMSynRM prototype project were of type Vacomax 255 HR with demagnetization heat tolerance up to 350 °C. The measurement results of temperature rise proved that PMSynRM has better thermal behavior than IM as if was expected. Due the good thermal behavior of PMSynRM, it can be overloaded for short periods without demagnetizing the permanent magnets in rotor. Measurement results also showed that PMSynRM is well suitable to operate with high efficiency in wide speed range and with a wide field weakening area.

REFERENCES

Aura, L. & A.J. Tonteri (1996). *Teoreettinen Sähkötekniikka ja sähkökoneidenperusteet*. Second edition. Helsinki. WSOY. 448 p. ISBN 951-0-21385-3.

ABB (2001) *Sähkökäytön mitoitus*. Technical guide no. 7. Available from the internet: <https://library.e.abb.com/public/b11d4fe92973be93c1256d2800415027/Tekninen_opasnro7.pdf> 40 p.

ABB (2004) *Permanent Magnet Motors*. Catalog. Available from the internet: <http://www.novec.ru/catalog/novosibirsk/catalog/abb/perm_drv.pdf> 72 p.

ABB (2012) *M3BJ -kestomagneettimoottorien ladonta ja kokoonpano*. Working instruction. Not available in public use.

ABB (2014a). *IEC 60034-30-1 standard on efficiency classes for low voltage AC motors*. Technical note. Available from the internet: <https://library.e.abb.com/public/1018a82e36b29462c1257d41002b3470/TM025%20EN%2008-2014%20IEC60034-30-1_lowres.pdf> 2 p.

ABB (2014b). *Low voltage motors*. Motor guide. Third edition. ISBN 952-91-0728-5. ABB Oy. 126 p.

ABB (2014c). *Low voltage Process performance motors according to Australian MEPS*. Catalog. Available from the internet: <<http://search.abb.com/library/Download.aspx?DocumentID=9AKK105944&LanguageCode=en&DocumentPartId=AU-EN&Action=Launch>>

ABB (2015a). *AC Induction low inertia motors High dynamic performance series*. Catalog. Available from the internet: <<https://search-ext.abb.com/library/Download.aspx?DocumentID=9AKK105767&LanguageCode=en&DocumentPartId=&Action=Launch>>

ABB (2015b). *Low voltage AC drives*. Catalog. Available from the internet: < https://library.e.abb.com/public/3d37392c24534d28b001fc8c0cd85646/3AUA0000139403_REVL.pdf >

ABB (2016). *Low voltage – IE4 synchronous reluctance motors*. Catalog. Available from the internet: <https://library.e.abb.com/public/6d4f5034141d4e0eb9f30a1abc6-445fc/IE4_SynRM_08-2016_LOW.pdf>

Bali, M., A. Muetze (2014). Influences of CO₂ and FKL-laser cutting as well as mechanical cutting on the magnetic properties of electric steel sheets determined by Epstein frame and stator lamination stack measurements. *IEEE Transaction on Energy Conversion Congress and Exposition (ECCE 2014)*, Pittsburgh, PA, USA, p. 1443–1450.

Cogent Power (2002). *Electrical Steel Non Oriented Fully Processed*. Catalog. Available from the internet: <<https://perso.uclouvain.be/ernest.matagne/ELEC2311/T2006/NOFP.pdf>>

Electronics Tutorials (2017). *Magnetic Hysteresis*. Available from the internet: <<http://www.electronics-tutorials.ws/electromagnetism/magnetic-hysteresis.html>>

Fratta, A., A. Vagati, F. Villata (1992). On the evolution of AC machines for spindle drive. *IEEE Transaction on Industry Applications*, Torino, Italy, 699–704

Gieras, J. F. & M. Wing (2002). *Permanent Magnet Motor Technology. Design and Applications Second Edition, Revised and Expanded*. New York: Marcel Dekker. 590 p. ISBN 0-8247-0739-7.

Haapala, T. (2011). *Measuring Cardiac Pacemakers and Implantable Cardioverter Defibrillators in a Substation and Under Power Lines*. Master of Science Thesis. Tampere University of technology. 73 p.

- Haataja, J. (2003). A comparative performance study of four-pole induction motors and synchronous reluctance motors in variable speed drives. Doctoral Thesis. *Acta Universitatis Lappeenrantaensis* 153, 138 p. Lappeenranta University of Technology. Lappeenranta, Finland. ISBN 951-764-772-7.
- Hirvelä, J. (2013). *Development of rotor for permanent magnet assisted synchronous reluctance rotor*. Master of Science Thesis. Vaasa University. Electrical Engineering. Vaasa, Finland. 91 p.
- Hyvönen, A. (2016). *Bearing currents in small squirrel cage motor*. Master of Science Thesis. Vaasa University. Electrical Engineering. 73 p.
- Khan, K.A. (2011). *Design of a Permanent-Magnet Assisted Synchronous Reluctance Machine for a Plug-In Hybrid Electric Vehicle*. Licentiate Thesis. Electrical Machines and Power Electronics School of Electrical Engineering, KTH. Stockholm, Sweden. ISBN 978-91-7601-166-0. 61 p.
- Kim, W.-H., K.-S. Kim, S.-J. Kim, D.-W. Kang, S.-C. Go, Y.-D. Chun, J. Lee (2009). Optimal PM design of PMA-SynRM for wide constant-power operation and torque ripple reduction. *IEEE Transactions on Magnetics* 45:10, 4660–4663.
- Kolehmainen J. (2011). Dovetail rotor poles in synchronous permanent magnet and reluctance machines. Doctoral Dissertation. *Aalto University publication series Doctoral Dissertations 60/2011*, 69 p. Aalto University, Department of Electrical Engineering. Espoo, Finland. ISBN 978-952-60-4195-7.
- Kolehmainen, J. (2012a). *Suunnittelu*. Presentation on 4 December, 2012 at the University of Vaasa. In Finnish. 20 p.
- Kolehmainen, J. (2012b). *Tahtireluktanssikone*. Presentation on 19 November, 2012 at the University of Vaasa. In Finnish. 31 p.

- Kolehmainen, J. (2017). *Laajan nopeusalueen käytöt – Drives for wide speed range*. Presentation on 20 February, 2017 at the University of Vaasa. In Finnish. 24 p.
- Krishnan, R. (2001). Switched Reluctance Motor Drives. In: *Industrial Electronics Series*, 398 p. Eds. J. David Irwin. Virginia: Virginia Tech. ISBN 0-8493-0838-0.
- Kärkkäinen, H., L. Aarniovuori, M. Niemelä, J. Pyrhönen (2017). Converter-Fed Induction Motor Efficiency: Practical Applicability of IEC Methods. *IEEE Industrial Electronics Magazine* vol. 11, no.2, p. 45–57.
- Lee, J.-Y., D.-K. Hong, B.-C. Woo, D.-H. Park, Y.-H. Choi, B.-U. Nam (2012). Unbalanced Magnetic Force Calculation for Rotor and Stator Assembly in Permanent Magnet Motor with Large Diameter. *Electromagnetic Field Problems and Applications, Sixth International Conference on (ICEF 2012)*, Dalian, Liaoning, China. 4p.
- Liu, H.-K., I.-G. Kim, Y.J. Oh, J. Lee, S.-C. Go (2017). Design of Permanent Magnet-Assisted Synchronous Reluctance Motor for Maximized Back-EMF and Torque Ripple Reduction. *IEEE Transactions on Magnetics*, vol. 53, no. 6, p. 1–4
- Luo, J., W. Zhao, J. Ji, J. Zheng, Y. Zhang, Z. Ling, J. Mao. (2017). Reduction of Eddy-Current Loss in Flux-Switching Permanent-Magnet Machines Using Rotor Magnetic Flux Barriers. *IEEE Transaction on Magnetics*, vol. 53, no. 11, p. 1–5
- Mahmoudi, A., W.L. Soong, G. Pellegrino, E. Armando (2015). Efficiency maps of electrical machines. *IEEE Energy Conversion Congress and Exposition (ECCE 2015)*, Montreal, QC, Canada, p. 2791–2799.
- Mohanarajah, T., J. Rizk, M. Nagrial, A. Hellany (2016). Comparative Analysis of Synchronous Reluctance Machines with and without Permanent Magnets. *IEEE International Conference on Power System Technology (POWERCON 2016)*, Wollongong, NSW, Australia, p. 1–6.

- Moghaddam, R.-R. (2011). *Synchronous Reluctance Machine (SynRM) in Variable Speed Drives (VSD) Applications*. Doctoral Thesis in Electrical Engineering. Royal Institute of Technology (KTH), Stockholm, Sweden. 260 p.
- Möttönen, N. (2013), *Life cycle assessment for two cast iron squirrel cage motor*, Master of Science Thesis. Vaasa University. Electrical Engineering. Vaasa, Finland. 173 p.
- Neorem Magnets (2014). *Permanent Magnets*. Product sheet. Available from the internet: <<http://www.neorem.fi/files/neorem/product-PDF/500a/neoremagneetikayrasmalli-a5-595a.pdf>>
- Piuhola, A. (2003), *Determination of Permanent Magnet Motor Losses and Temperature Rise*. Master of Science Thesis. University of Oulu, Oulu, Finland. 85 p.
- Pyrhönen, J, T. Jokinen, V. Hrabovcova (2014). *Design of Rotating Electrical Machines*. Second edition. West Sussex: John Wiley & Sons. 584 p. ISBN 978-1-118-58157-5.
- Ryppö, E. (2005). *Optimization of The Rotor Structure of an Induction Motor with Distributed Computing*. Master of Science Thesis. Helsinki University of technology. Electrical engineering. Espoo, Finland. 51 p.
- Salminen, P. (2014). Fractional slot permanent magnet synchronous motors for low speed applications. Doctoral Thesis. *Universitatis Lappeenrantaensis* 198, 152 p. Lappeenranta University of Technology. Lappeenranta, Finland. ISBN 951-764-982-7.
- Shin, S., Kim, J., Lee, S. B., Lim, C., Wiedenbrug, E. J. (2015). Evaluation of the Influence of Rotor Magnetic Anisotropy on Condition Monitoring of Two-Pole Induction Motors. *IEEE Transaction on Industry Applications*. vol. 51, no. 4, p. 2896–2904
- Söderang, E. (2016), *Analytical Dynamic Thermal Model for Squirrel Cage Motors Using Systemmodeler*. Master of Science Thesis. Vaasa University. Electrical Engineering. Vaasa, Finland. 134 p.

Talvitie, T. (2005). *Adaption and Utilisation of FEM-software to fast Permanent Magnet Synchronous Machine Designing*. Master of Science Thesis. Tampere University of Technology. Institute of Electromagnetics. Tampere, Finland 84 p.

The Engineering Toolbox. Available from the internet: <https://www.engineeringtoolbox.com/permeability-d_1923.html>

United Nations Framework Convention on Climate Change. 2015. Paris agreement. 12.12.2015. Available from the internet: <https://unfccc.int/files/essential_background/convention/application/pdf/english_paris_agreement.pdf>

VAC (2014). *Rare Earth Permanent Magnets*. Brochure. Available from the internet: <http://www.vacuumschmelze.com/fileadmin/Medienbibliothek_2010/Downloads/DM/Vacodym-vacomax-PD002_2015_en.pdf> 72 p.

Vesti, J. (2013). *Utilization of Copper Rotor in High Efficiency Induction motor*. Master of Science Thesis. Vaasa University. Electrical Engineering. Vaasa, Finland. 83 p.

Wang, Y., N. Bianchi, S. Bolognani, L. Alberti (2017). Synchronous motors for traction applications. *International Conference of Electrical and Electronic Technologies for Automotive (EETA 2017)*, Torino, Italy, 8 p.

Woo D.-K., S.-Y. Lee, J.-H. Seo, H.-K. Jung (2008). Optimal rotor structure design of interior-permanent magnet synchronous machine base on improved niching genetic algorithm. *18th International Conference on Electrical Machines (ICEM 2008)*, Vilamoura, Portugal, 4 p.

APPENDICES

Appendix 1. Efficiency classes based on IEC standard 60034-30-1 (ABB 2014a).

Super-Premium efficiency	IE4
Premium efficiency	IE3
High efficiency	IE2
Standard efficiency	IE1

IE efficiency classes for 4 pole motors at 50 Hz

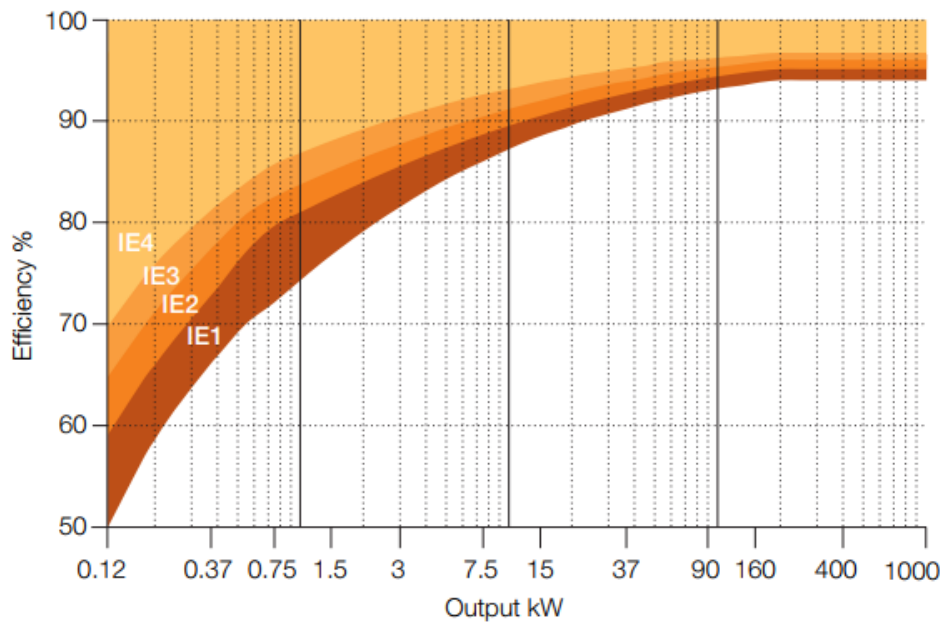


Figure 56. Efficiency classes of electric motors based on IEC standard 60034-30-1.

Appendix 2. Two-dimensional drawing of PMASynRM 250 prototype rotor sheet, designed by Jere Kolehmainen, ABB Motors and Generators, Vaasa.

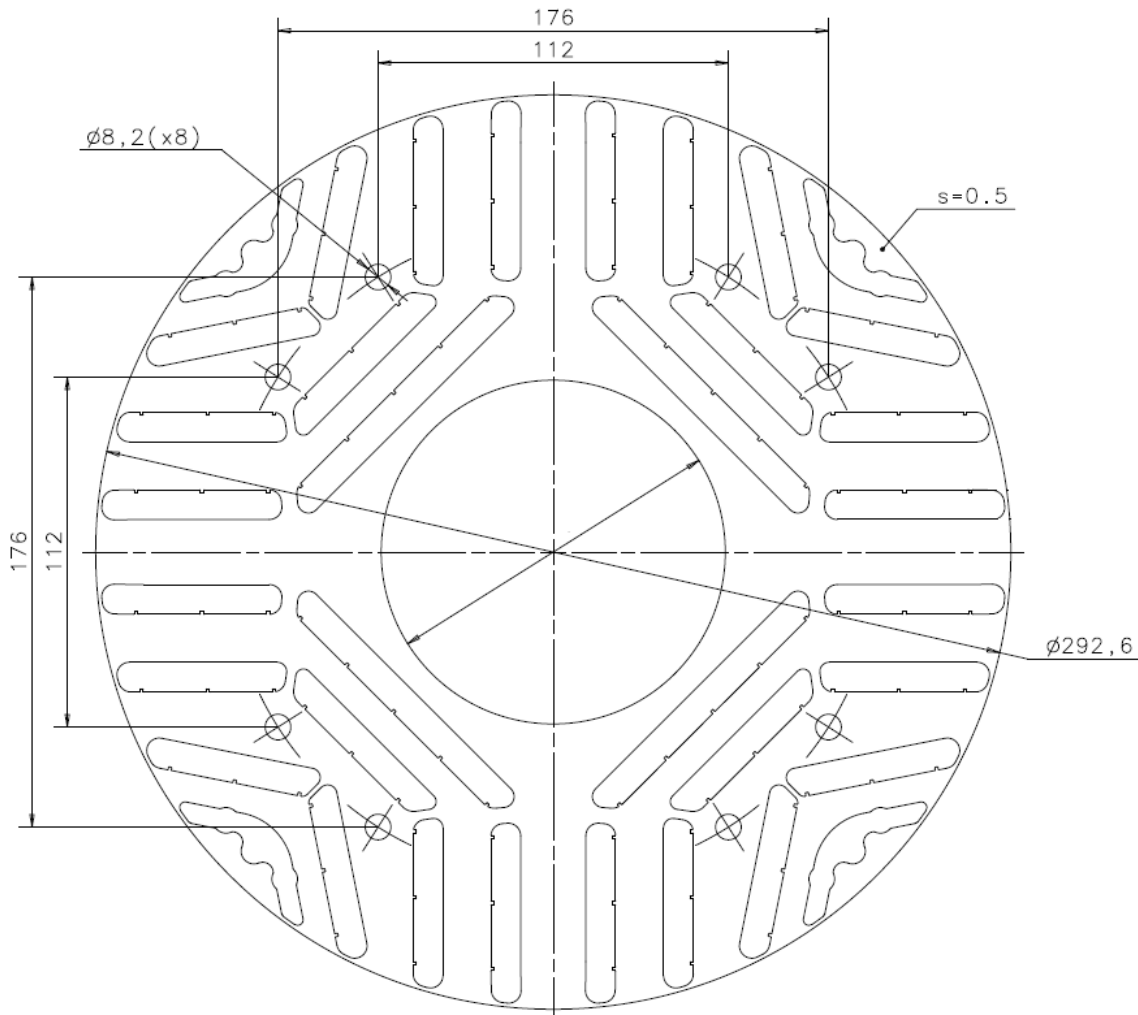


Figure 57. Two-dimensional drawing of PMASynRM 250 prototype rotor sheet.

Appendix 3. Common values for permeability (The Engineering Toolbox).**Table 7.** Common values for permeability and relative permeability. Modified from (The Engineering Toolbox).

Medium	Permeability (H/m)	Relative permeability
Air	$1.25663753 \cdot 10^{-6}$	1.00000037
Aluminum	$1.256665 \cdot 10^{-6}$	1.000022
Austenitic stainless steel	$1.260 \cdot 10^{-6}$ – $8.8 \cdot 10^{-6}$	1.003^{-7}
Bismuth	$1.25643 \cdot 10^{-6}$	0.999834
Carbon Steel	$1.26 \cdot 10^{-4}$	100
Cobalt-Iron	$2.3 \cdot 10^{-2}$	18000
Copper	$1.256629 \cdot 10^{-6}$	0.999994
Ferrite (nickel zinc)	$2.0 \cdot 10^{-5}$ – $8.0 \cdot 10^{-4}$	16 – 640
Ferritic stainless steel (annealed)	$1.26 \cdot 10^{-3}$ – $2.26 \cdot 10^{-3}$	1000 – 1800
Hydrogen	$1.2566371 \cdot 10^{-6}$	1
Iron (99.8 % pure)	$6.3 \cdot 10^{-3}$	5000
Iron (99.95 % pure)	$2.5 \cdot 10^{-1}$	200000
Martensitic stainless steel (annealed)	$9.42 \cdot 10^{-4}$ – $1.19 \cdot 10^{-3}$	750 – 950
Martensitic stainless steel (hardened)	$5.0 \cdot 10^{-5}$ – $1.2 \cdot 10^{-4}$	40 – 95
Nanoperm	$1.0 \cdot 10^{-1}$	80000
Neodymium magnet	$1.32 \cdot 10^{-6}$	1.05
Nickel	$1.26 \cdot 10^{-4}$ – $7.54 \cdot 10^{-4}$	100 – 600
Permalloy	$1.0 \cdot 10^{-2}$	8000
Platinum	$1.256970 \cdot 10^{-6}$	1.000265
Sapphire	$1.2566368 \cdot 10^{-6}$	0.99999976
Superconductors	0	0
Teflon	$1.2567 \cdot 10^{-6}$	1

Appendix 4. ABB ACS880-17-1950A-7 technical data (ABB 2015b).

ABB ACS880-17-1950A-7 main connection:

- 3-phase nominal voltage is 525–690 V, ± 10 %
- Frequency 50/60 Hz ± 5 %
- Efficiency at nominal power 97 %

ABB ACS880-17-1950A-7 motor connection:

- Motor control is direct torque control (DTC)
- Frequency is 0 to ± 500 Hz

ABB ACS880-17-1950A-7 nominal ratings:

- Power ratings are valid at nominal voltage 575 V
- Light-duty use (110 % overload for 1 minute every 5 minutes) current 1872 A and power 1900 kW
- Heavy-duty use (150 % overload for 1 minute every 5 minutes) current 1459 A and power 1400 kW